# EFFICIENT FINITE ELEMENT MODELING

# ACROSS OPTICAL LENGTH SCALES

by

Jason Alan Harwood

A thesis submitted in partial fulfillment
of the requirements for the degree

of

Master of Science

in

Mechanical Engineering

MONTANA STATE UNIVERSITY
Bozeman, Montana

May 2007

APPROVAL

of a thesis submitted by

Jason Alan Harwood

This thesis has been read by each member of the thesis committee and has been found to be satisfactory regarding content, English usage, format, citations, bibliographic style, and consistency, and is ready for submission to the Division of Graduate Education.

Dr. Christopher H. Jenkins

Approved for the Department of Mechanical and Industrial Engineering

Dr. Christopher H. Jenkins

Approved for the Division of Graduate Education

Dr. Carl A. Fox, Vice Provost

# STATEMENT OF PERMISSION TO USE

In presenting this thesis in partial fulfillment of the requirements for a master's degree at Montana State University, I agree that the Library shall make it available to borrowers under rules of the Library.

If I have indicated my intention to copyright this thesis by including a copyright notice page, copying is allowable only for scholarly purposes, consistent with "fair use" as prescribed in the U.S. Copyright Law. Requests for permission for extended quotation from or reproduction of this thesis in whole or in parts may be granted only by the copyright holder.

Jason Alan Harwood

May 2007

# ACKNOWLEDGEMENTS

I thank Dr. Christopher H. Jenkins for this research assistantship, funded through a small business grant from the Arnold Engineering Development Center, for the last two years and his continual support throughout my Master's program. In addition, I would like to thank Mr. Paul Gierow, CEO of GATR Technologies in Huntsville, Alabama and Primary Investigator for this project, for contracting MSU, and providing an opportunity travel to AEDC and be involved with the Phase I presentation of the project. I thank Dr. David Klumpar, Dr. Ladean McKittrick and Dr. Stephen Sofie, for serving on my graduate committee and Dr. Doug Cairns and Dr. Sofie and Dr. Robert Badaliance for their help and guidance during my research. I also greatly appreciate the donation of samples from Cytec Engineered Materials and Lattice Materials to help with my work. Finally, thanks to the staff and colleagues in the Mechanical and Industrial Engineering department for their help and support.

TABLE OF CONTENTS

TABLE OF CONTENTS - CONTINUED

# LIST OF TABLES

Table Page

# LIST OF FIGURES

LIST OF FIGURES - CONTINUED

# LIST OF EQUATIONS

# ABSTRACT

Optical engineers frequently rely on finite element analysis (FEA) to predict the thermal and mechanical performance of an optic before it is produced. These analyses are usually performed by modeling a simplified version of the real structure to obtain the global deformations of the surface of the mirror. This method eliminates the ability to represent localized deformations and strain gradients, resulting from thermal and mechanical loading, which may exceed the mechanical limit of the materials or material interfaces in coated mirrors causing delamination or cracking. The goal of this study is first to improve optical performance modeling by incorporating localized strain behavior within material layers and at material interfaces, bond strengths between mirror coatings and substrates, gravitational deformations, and effects of size scaling on deformation and strain magnitudes. Second, these methods will be used to investigate viability for constructing a coated mirror with mismatched coefficients of thermal expansion (CTE) with an interlayer of a polymer with a designable CTE to improve thermal deformation and reduce the risk of structural failure.

Modeling localized regions of an optic requires incorporating length scales differing by nine orders of magnitude. In order to precisely predict localized effects of the loading conditions, combinations of shell and continuum elements were used to minimize model size and computational time while localized accuracy is retained. Tie constraints were used to connect different elements and meshes and zero-thickness cohesive zones were created to predict delamination at material interfaces. Material properties for each material were specified to appropriate regions within the model, enabling realistic representation of deformation within mirror layers. This process was demonstrated on 3-D and axisymmetric models of a three-component mirror comprised of a coating, substrate, and an intermediate polymer layer with a designable CTE. Deformation and strain results were shown to change as the intermediate layer CTE was varied. Inclusion of the polymer layer was shown to have a slight effect on deformation resulting from gravity loading. Cohesive zone modeling techniques were used to investigate the strength of material interfaces after qualitative experimental verification. Parametric studies performed using axisymmetric cohesive zone models show that delamination resistance can be improved by tuning the polymer CTE.

.

# 1. INTRODUCTION

As the demand grows for lighter, higher-performing optics, optical engineers more frequently rely on finite element analysis (FEA) to help predict the thermal and mechanical performance of mirrors long before the optic is ever produced. Current FEA is usually performed by modeling a simplified version of the real structure and then loading the model thermally and/or mechanically. These global models often leave out the smaller features of the structure that would require finer meshes and more complicated models. The objective of the present study is two fold. First, to improve optical performance modeling by incorporating the following details in a finite element model:

1. Strain behavior within the layers and at material interfaces of the optic
2. Bond strengths between reflective and protective coatings and substrates
3. Gravitational effects
4. Scaling effects of larger mirrors on maximum stress/strain and deformed shape

All of these details can be accomplished simultaneously by using tools and features available in most major FEA software packages.

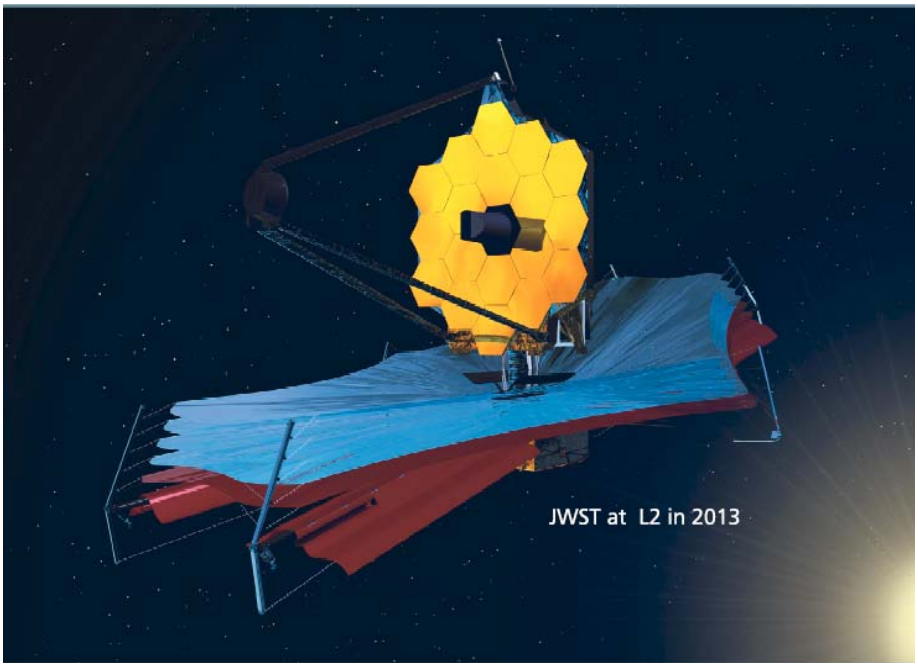


Figure 1. A rendition of the James Webb Space Telescope in its L2 orbit. The JWST project has used FEA extensively to model the optical performance of the mirror and thermomechanical performance of the supporting structure. Courtesy of NASA.

The second objective is to investigate the viability of building a coated optic using coating and substrate materials with mismatched CTE that also includes an interlayer of a polymer with a tunable CTE to improve thermal deformation and reduce the risk of structural failure. The tunable CTE of the polymer helps distribute the strain mismatch between the coating and the substrate. By doing so, exceeding the material limits of the coating and substrate materials during thermal cycling can be avoided as well as reducing the possibility of delamination by reducing the strain mismatch at material interfaces.

# 2. BACKGROUND

At the Arnold Engineering Development Center, Arnold AFB, TN, two cold chambers are used to provide sensor calibration, high-fidelity mission simulation and hardware-in-the-loop simulation in a low infrared, vacuum environment. The chambers operate at a temperature of approximately 20 K and a pressure on the order of $10^{-6}$ torr [Lowry et al., 2005-a; Lowry et al., 2005-b]. Both chambers contain a sophisticated optical system comprised of several mirrors, attenuators, beam splitters, and combiners, as well as other optical equipment. Each component was designed for optimum optical performance with respect to reflection (or transmission), thermal distortion and longevity.

Figure 2. The 7V and 10V optical chambers at AEDC on the left and right respectively.

As a result of the necessity for high reflectivity, special coatings are often applied to the mirror substrates. These coatings often have different coefficients of thermal expansion (CTE) than the substrates, and because the mirrors operate at such a low temperature, distortion of the surface figure and catastrophic failure of the coating are common concerns. (Failure of this type is documented in the article by Lowry et al., 2005-a). FEA is frequently

used to estimate the deformed surface figure, but it is used less to analyze the localized stresses caused by the CTE mismatch of a globally deformed mirror. This evaluation is necessary, along with including the mechanical limits of the materials and bonds between materials, to predict the onset of delamination or cracking. Analyzing the local stresses usually means a much finer mesh must be used as a result of the difference in scale between the substrate and coatings. Consequently, the strain state at material interfaces or the boundary of the mirror is unknown because of the coarse meshes used for global deformation.

Because an optic with mismatched CTE will deform regardless of the precautions taken, one option to minimize the deformation is to match the CTE of the components through material selection. CTE matching by material selection works well if the substrate material is compatible with the coating and coating process. Consequently, low CTE materials are often chosen for the substrate anyway to minimize distortion resulting from thermal gradients through the structure. Choosing low or matched CTE materials for a coating and substrate may not always be a viable option, however. In the case of the chambers at AEDC, the optical bench is constructed of aluminum and contracts as the chamber is cooled. If the mirrors are also made of aluminum, or one with a similar CTE, everything remains in focus during cool down and setup is much easier. Aluminum has excellent spectral properties but, unfortunately, has a high CTE and slowly grows an oxide layer when exposed in most environments that reduces performance. [Lowry et al., 2005-a] This means that some sort of coating is necessary and thermal cycling may cause distortion, delamination, and/or cracking of the optic.

If material selection does not lead to a satisfactory option, material engineering may be an option. Modifying thermal properties of materials, especially polymers and composites, by doping them with other elements and compounds is being researched by several companies. The goal is to reduce or match the CTE of materials for improved optical and mechanical performance in optics, miniature electro-mechanical, and electro-optical devices. As a result, the thermal strains resulting from manufacture or operation are reduced. One problem, however, briefly mentioned in Section 7, is the effect this type of doping has on mechanical performance.

In the case of AEDC, material engineering of the substrates and coatings is not much of an option. However, GATR Technologies (Huntsville, Alabama) has suggested that engineering a material to mitigate the strain mismatch between the coatings and substrates desired by AEDC is promising. Modifying the CTE of polymers has been successfully demonstrated by SRS Technologies (Huntsville, Alabama) using their proprietary Novastrat® polyimides. By adding the polymer interlayer to optics, the strain mismatch can be distributed through the thickness of the more compliant material, reducing the potential for mechanical failure of the coating.

# 3. LITERATURE REVIEW

As imaging technology advances, the need for better performing optics increases, and the environments that optics are expected to perform in also become increasingly harsh. Advanced coating materials and processes are used to increase reflectivity and new substrate materials are used to make stiffer, lighter mirrors. Tolerances on surface figures and smoothness are more stringent. In addition, the thermal demands that optics are subjected to become increasingly severe as more imaging is performed in cold environments such as space and infrared testing systems, where temperatures and pressures are extremely low. Finite element analysis is being used more frequently as a tool to examine the effects of thermal and mechanical loading on these technically advanced structures.

## Coatings

Coatings used in optical applications usually pose problems for designers. The coatings are applied to mirror substrates to achieve optical performance, e.g., in reflectivity or polarization. Frequently, these coatings have drastically different thermal expansion coefficients (CTE) and elastic moduli than the substrates they are applied to. The combination of mismatched CTE and stiffness may cause distortion of the surface figure or mechanical failure of the optic when subjected to changes in thermal environment. The degree of distortion is related to many factors including the thickness of the coating, the shape of the substrate, the magnitude of CTE mismatch, and type of thermal environment to which the optic is subjected.

In his dissertation, Moon (2001) analyzed the effects of several combinations of these factors. Coated mirrors were modeled using the finite element program SDRC I-deas by meshing a substrate of solid elements with a layer of plate elements representing the coating. Various substrate shapes were modeled with two different substrate/coating material combinations. Each shape/material was subjected to a variety of thermal conditions, such as thermal soak, radial temperature distributions, and axial temperature distributions. The purpose of the dissertation was to characterize the effects of different thermal and geometric conditions and relate them to analytical models. Though focusing primarily on distortion rather than mechanical failure, Moon's work provides an important example of the use of different element types to model across the dimensional scales of the coating and substrate.

Problems resulting from thermal expansion mismatch are not limited to optical structures. Delamination and cracking occurs in electronic chips resulting from thermal processing during manufacture and different CTEs of the materials used to construct and package the chips. Finite element analysis was used on micrometer-scale devices to analyze fracture film cracking and delamination [He et al., 2005]. The work indicates global and local CTE mismatches are responsible for film cracking and delamination.

The process used to apply coatings to optics and other devices has bearing on the amount of thermal mismatch that can be present in a structure as well as the amount of residual strain that remains in the coating after high temperature processing. When investigating plasma deposited silicon nitride films used for microsystems, it was found that residual strain in films was dominated by the thermal mismatch of the materials [Soh et al., 2005]. This conclusion means that residual strain that remains after deposition is due to the

high temperatures used to create the film and the significant difference between manufacture and operating temperatures. So, not only is the CTE of materials a factor of performance during operation, it may also be a factor in residual strains resulting from deposition, leading to further reduced performance or failure. Also, it was noted that film CTE is a function of deposition temperature and that lower deposition temperatures lead to an increase in CTE [Soh et al., 2005]. Though not discussed in the present study, future work may need to address changes in material properties resulting from processing conditions.

## Finite Element Modeling of Optics

Difficulties arise when modeling coated optics with FEA. Most obvious is the drastic change in scale between the coating thickness and the dimensions of the substrate. Usually mirrors are on the order of several millimeters to several centimeters thick with diameters from a few centimeters to a few meters. This gives a thickness to width ratio of approximately 1/1000. However, optical coatings are frequently ten to several hundred nanometers thin. This means that coating thickness to mirror width ratios can differ by seven orders of magnitude or more. This can cause obvious problems for element size, shape and, mesh density. To avoid this problem, several methods have been used.

As already mentioned, Moon used two different elements to represent the different parts of the mirrors being modeled [Moon, 2001]. By representing the coating with plate elements, the thin dimension of the coating is avoided, and a relatively coarse mesh can be used to accurately predict the response of the model. This is much more efficient

computationally compared to the very dense mesh needed if the entire model were meshed with solid elements.

Kendrew et al. (2006), chose to take advantage of the element definitions used for composite modeling. Composite element definition allows each element to contain several layers of different materials, thicknesses, and orientation. Their example of this method was demonstrated at the University College London on a design for an actively controlled composite mirror. In the analysis, a carbon fiber lay-up sandwiching a core of honeycomb aluminum with a nickel coating was modeled using Ansys/Nastran and I-deas and using the *Laminates* tool.

Both of these methods were compared in a parametric analysis by Doyle et al. (2002). The analysis compared three different approaches to use FEA to study the problems of CTE mismatches, Twyman effects, and moisture absorption. These three approaches were labeled the composite plate model, the homogeneous plate model, and the 3-D model [Doyle et al., 2002]. The composite plate model was similar to that used by Kendrew et al., (2006). The homogeneous plate model used plate elements but avoids the composite lay-up by averaging the material properties to find effective material properties for the lay-up. (This is necessary when the available software does not support composite element definition.) The 3-D model was similar to that used by Moon (2001), where plate elements were meshed on the surface of 3-D elements. Doyle et al. (2002) concluded that each method has advantages of accuracy and efficiency depending on the needs of the analysis and the tools available. Both the composite method and a modified version of the 3-D method are used in the present analysis.

## Cohesive Zone Modeling

Cohesive zone modeling is a type of FEA modeling that uses specially defined elements to model crack initiation and progression. Cohesive zone modeling avoids the need for the seeding of cracks in a model and the moving mesh required to model crack progression if Virtual Crack Closure or J-Integral techniques are used [Meo and Thieulot, 2005].

A variety of delamination modeling methods are compared in the work done by Meo and Thieulot (2005). In their work, they modeled a double cantilever beam to evaluate mode I fracture using four different techniques: cohesive zone modeling, nonlinear springs, birth and death of elements, and tie-break contact. The results of this work show that cohesive zone modeling is a good way to model crack initiation and propagation. Though it was not the best method in the study, further mesh refinement or better response definition could be used to improve the correlation between numerical and experimental data.

Cohesive zone models, particularly in ABAQUS, can be defined using two methods [ABAQUS 6.5 documentation, 2004]. First, the cohesive zone can be defined using typical material properties in regions with finite dimensions. The response of the material is calculated based on the geometry of the region and the assigned material properties. Damage initiation and damage evolution can then be defined for the cohesive elements according to the stress and/or strain imposed on the elements. Damage initiation occurs when the element reaches a stress or strain state that exceeds a criterion specified by the user corresponding to the material or material interface being modeled. From this point, the element begins to

degrade according a damage evolution law also specified by the user. The user also defines when the element is totally degraded. A typical stiffness verses loading curve for a model defined with damage initiation and linear degradation law is shown in Figure 3 [ABAQUS V.6.5 documentation, 2004; Meo and Thieulot, 2005].

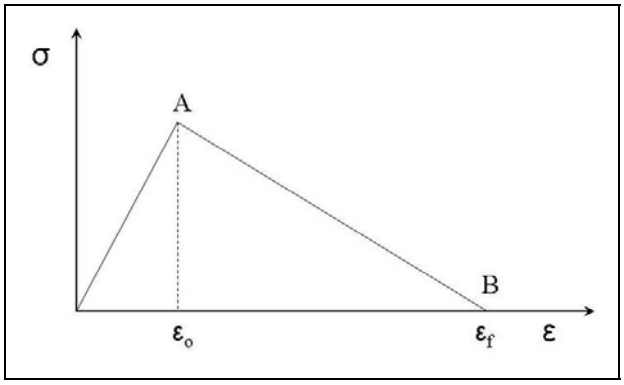


Figure 3. Bilinear softening model for damage evolution. For $\varepsilon < \varepsilon_o$, the material exhibits an elastic response. At *A*, damage is initiated and further loading causes the material to soften for $\varepsilon_o < \varepsilon < \varepsilon_f$. At *B*, the material has been completely damaged and separated.

Unaltered material response occurs before *A*. At *A*, damage is initiated and damage evolution begins. As the element continues to be loaded, the stiffness of the element degrades until it becomes negligible at *B*, where the element stiffness is totally degraded. The element can then be removed from the analysis, if desired.

The second method for defining cohesive zones is based on traction and separation response. This method is used when the zone has a very small or zero thickness. Instead of using the geometry to calculate the stiffness of the cohesive elements, the stiffness is defined in traction and separation stiffnesses. A unit thickness is assumed for internal calculations for strain so that the reported strain is equal to the actual deflection. The matrix equation, showing how strain is calculated from applied stress and traction stiffnesses is shown below

as Equation 1. Damage initiation is still defined in the same manner in terms of stress or strain as well as damage evolution [ABAQUS V.6.5 Documentation, 2004].

$$\mathbf{T} = \begin{Bmatrix} t_n \\ t_s \\ t_t \end{Bmatrix} = \begin{bmatrix} K_{nn} & 0 & 0 \\ 0 & K_{ss} & 0 \\ 0 & 0 & K_{tt} \end{bmatrix} * \begin{pmatrix} \varepsilon_n \\ \varepsilon_s \\ \varepsilon_t \end{pmatrix} = \mathbf{K} * \mathbf{E} \qquad (1)$$

Equation 1 is the matrix equation used to calculate stresses or strains in cohesive elements with an uncoupled traction-separation element definition. T is the traction (or stress) vector with one normal and two shear components. E is the separation (or strain) vector, also with on normal and two shear components. K is the stiffness matrix defined in the cohesive material definition with one normal and two shear components [ABAQUS V.6.5 Documentation, 2004].

# 4. FINITE ELEMENT MODELS

Several different finite element models were used for investigation of layered mirror behavior. Two axisymmetric models and one 3-D model were used to investigate the optical performance of a mirror with a polymer interlayer and compared to a mirror without the polymer interlayer. These models were used to study a variety of aspects of optical design such as deformation and elastic strain due to thermal loading, intrinsic coating stress, scaling effects of larger mirrors on strain and surface figure, deformation due to gravity.

All models consisted of a coating layer, a substrate layer, and a polymer layer between the coating and substrate. The polymer layer was omitted from a few models when only the effects of a substrate and coating were desired for comparison. In general, the thickness of the polymer was 0.02 mm except a for a few trials and the CTE of the polymer was varied between $5 \times 10^{-6}$ and $25 \times 10^{-6}$ $^{mm}/_{mm \cdot ^{o}C}$, the estimated CTE of the coating and bulk aluminum, respectively. In these analyses, the total strain is the sum of the thermal strain and the elastic strain. Each material layer experienced some amount of contraction, or thermal strain, due to cooling, however, the adhesive and coating layers were also strained mechanically by the thermal deformations of the stiffer substrate a higher CTE. For these reasons, mechanical strain within the substrate was very low compared to the other layers.

## Composite Shell Model

The composite shell model was created using 3500 SAX2T 3-node, quadratic, axisymmetric shell elements with temperature degrees of freedom. The properties of the elements were assigned using a composite material definition. This allows the material properties of an element to be assigned in layers, as would be done for modeling of composite structures. Material properties, such as CTE and Young's Modulus, as well as geometric and numerical properties, such as thickness, orientation, and number of integration points, can be assigned to each layer independently. Element properties, like stiffness for example, are then calculated according to the material definition by combining all layers in each element. A schematic of the composite shell model is displayed below in Figure 4 with the material properties used for each layer.

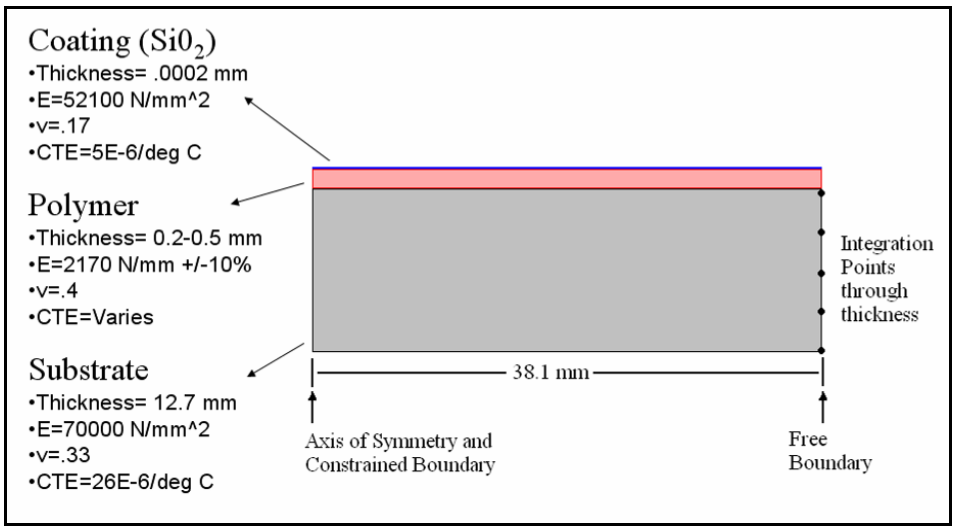


Figure 4: Composite shell model schematic. Each element in the composite shell model contains the three layers labeled above. Integration points are spaced as shown in the substrate layer for computation purposes and to extract data, however, there remains one element through the thickness and the number of integration points was limited to 20 per element.

Using these elements, output variables such as stress, strain, and displacement could be output at nodal locations or at Gaussian integration point locations. Though the number of integration points could be specified for a layer, the total number of integration points was limited by the software to twenty integration points per element and only one element represented all layers through the thickness. Nodal quantities of stress and strain are the averaged values of the integration point quantities taken through the thickness. For this reason, data collected using this model was output at the integration points to determine how strain varied between the layers of the model. An example of the data from this model is shown in Figure 5. The CTE, elastic modulus and thickness of the polymer layer vary between trials in order to determine the dependence of thickness and CTE on radial strain mismatch. As a result of the nature of the composite elements, strain through the thickness does not vary with respect to radius.

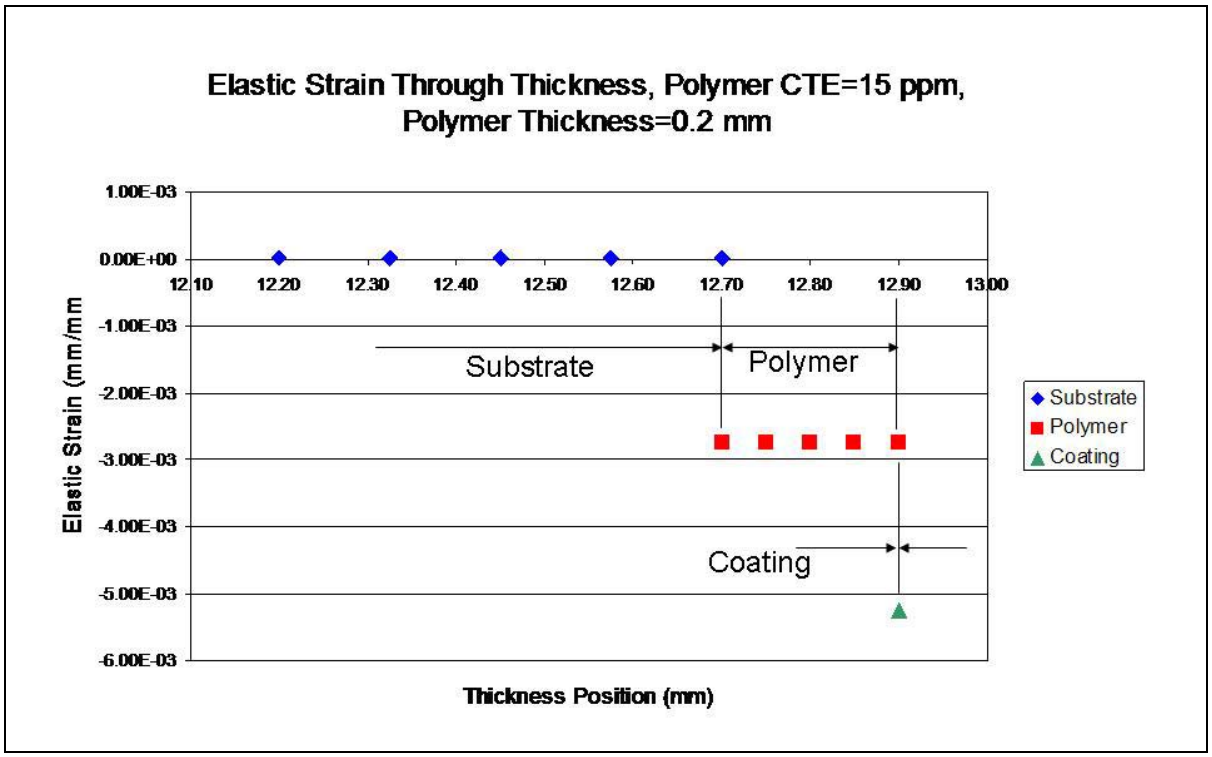


Figure 5: Typical data output at integration points. Note that an extra layer in the substrate was included to provide additional refinement for analyzing the strain state near the polymer layer. In all, a total of twenty integration points were used in each element, ten in the two layers of the substrate, and five each in the polymer and coating layers.

Because the deformations are calculated only at the nodes, the magnitude of total strain is equal in all layers. Elastic strain is constant within each layer and changes between layers as a result of differences in thermal strain caused by the various CTE values. This revealed some of the limitations of the composite shell model and the motivation to develop a more sophisticated model. These limitations include: the ability to represent deformation within a layer, resolution of strain gradients within the layer, and calculation of additional variables such as shear strain. However, some trends could be extracted from the composite shell model.

Table 1 summarizes the strain mismatch results from various combinations of polymer CTE and polymer thickness. In all cases, the strain mismatch between the coating and substrate layers had a magnitude of $5.25 \times 10^{-5}$ $^{mm}/_{mm}$. Depending on the CTE of the polymer, this mismatch was distributed between the polymer/coating interface and the polymer/substrate interface. For example, if the polymer CTE matched the CTE of the coating, there was zero strain mismatch at that interface and the strain mismatch at the polymer/substrate interface was $5.25 \times 10^{-5}$ $^{mm}/_{mm}$. Likewise, if the polymer CTE matched the CTE of the substrate, there was zero strain mismatch at that interface and the strain mismatch at the polymer/coating interface was $5.25 \times 10^{-5}$ $^{mm}/_{mm}$. If the magnitude of polymer CTE was between that of the substrate and the coating, the mismatch was proportionately distributed between the two respective interfaces. This means that although the polymer layer does not eliminate mechanical strain mismatch, it can be used to distribute the strain difference from one interface to the other, either partially or fully. Therefore, the level of strain at an interface could potentially be reduced below the critical value and prevent failure. Although the strain mismatch between materials is independent of the polymer thickness, the strain gradient, or shear strain, within the polymer layer is dependent on polymer thickness and would need to be investigated if damage occurs within the polymer layer. It is also worth noting that the magnitude of strain is independent of the location along the radius of the model.

Table 1: a. Mechanical strain values and mismatch results at material interfaces from composite shell model including the polymer. b. Strain values and mismatch results at material interfaces from the composite shell model excluding the polymer. It is important to note that the total magnitude of strain mismatch between the coating and substrate is constant despite the CTE of the polymer. By adding the polymer and varying the CTE, the mismatch is simply distributed between the interfaces. E is the elastic modulus and h is the polymer thickness.

a.

| Strain Values and Mismatch at Interface | | | | | | |
|---|---|---|---|---|---|---|
| Polymer Properties CTE / E / h $deg^{-1}$ C / $N/mm^2$ / mm | Polymer Strain | Coating Strain | Polymer/ Coating Strain Mismatch | Substrate Strain | Polymer Strain | Substrate/ Polymer Strain Mismatch |
| 2 / 2170 / 0.2 | -5.99E-03 | -5.24E-03 | **-7.50E-04** | 1.34E-05 | -5.99E-03 | **6.00E-03** |
| 2 / 2170 / 0.5 | -5.96E-03 | -5.21E-03 | **-7.50E-04** | 3.37E-05 | -5.97E-03 | **6.00E-03** |
| 5 / 2170 / 0.02 | -5.25E-03 | -5.25E-03 | **0.00E+00** | 1.35E-06 | -5.25E-03 | **5.25E-03** |
| 5 / 2170 / 0.2 | -5.24E-03 | -5.24E-03 | **0.00E+00** | 1.18E-05 | -5.24E-03 | **5.25E-03** |
| 5 / 2170 / 0.5 | -5.22E-03 | -5.22E-03 | **0.00E+00** | 2.95E-05 | -5.22E-03 | **5.25E-03** |
| 5 / 2170-10% / 0.2 | -5.24E-03 | -5.24E-03 | **0.00E+00** | 1.06E-05 | -5.24E-03 | **5.25E-03** |
| 5 / 2170+10% / 0.2 | -5.24E-03 | -5.24E-03 | **0.00E+00** | 1.29E-05 | -5.24E-03 | **5.25E-03** |
| 15 / 2170 / 0.2 | -2.74E-03 | -5.24E-03 | **2.50E-03** | 6.26E-06 | -2.74E-03 | **2.75E-03** |
| 15 / 2170 / 0.5 | -2.73E-03 | -5.23E-03 | **2.50E-03** | 1.56E-05 | -2.73E-03 | **2.75E-03** |
| 26 / 2170 / 0.2 | 2.08E-07 | -5.25E-03 | **5.25E-03** | 2.03E-07 | 2.03E-07 | **0.00E+00** |
| 26 / 2170 / 0.5 | 2.22E-07 | -5.25E-03 | **5.25E-03** | 2.09E-07 | 2.09E-07 | **0.00E+00** |

b.

| Without Polymer | Substrate Strain | Coating Strain | Substrate/ Coating Strain Mismatch |
|---|---|---|---|
| | 1.99E-07 | -5.25E-03 | **5.25E-03** |

Though some important conclusions can be made using the composite shell model and it was fairly simple to create, there are some very limiting shortcomings to the model. First, because all layers are contained in one element and deformations within each layer are constrained to the same node, the layers cannot deform with respect to each other. Despite the edge of the mirror being smooth and hence edges of the layers being flush, there will be a stress concentration at the interfaces of the materials where the material properties abruptly

change. The composite shell model does not allow insight into the deformations and stress/strain results caused by the abrupt change in materials. Also, it is not easily possible to apply intrinsic coating stresses to the model. This ability is important because often coatings have high levels of intrinsic stress, either compressive or tensile, after deposition and/or curing. These stresses can have a very significant effect on the performance and durability of the mirror. Finally, because being able to predict the figure of the mirror is important to any optical analysis, representative geometry of the actual structure is essential for precise prediction of the optic's deformations. This level of detail is not attainable with a shell model. Consequently, a more sophisticated model must be created.

## Hybrid Model

The hybrid model was created using a combination of 7000 SAX2T axisymmetric shell elements and 14,500 CAX8T axisymmetric continuum elements, all with temperature degrees of freedom. Because the length scales of the coating and substrates vary by upwards of nine orders of magnitude, creating a mesh composed completely of continuum elements that will provide sufficient detail is not feasible. For this reason, a layer of shell elements were tied to the top of a section of continuum elements and another layer of shell elements were tied to the bottom of the section of continuum elements. The Tie Constraint that was used in ABAQUS forces the elements constrained to move together. Tie constraints are useful in situations where rapid changes in mesh density are required, or in this case, where element types are different. (ABAQUS 6.5 documentation). In doing so, it was possible to

zoom in with the continuum elements on the entire polymer layer and a small portion of the substrate. A schematic of the hybrid model is shown below in Figure 6.

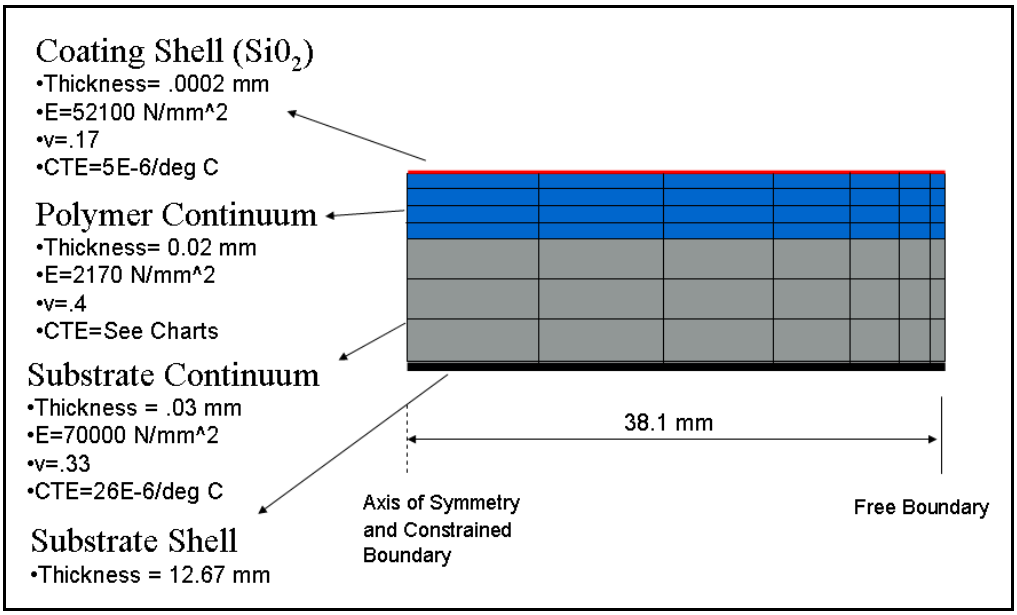


Figure 6: Hybrid model schematic. The element size was biased from the axis of symmetry to the free boundary to minimize the number of elements and improve convergence in the strain result at the edge.

The geometry of the hybrid model is consistent with the geometry of the composite shell model so that the results of two models could be compared and validated with respect to one another. A characteristic result of the hybrid model is shown below along with a comparison of the strain results between the hybrid model and the composite model in Figure 7 and Figure 8, respectively. The polymer layer is distorted significantly at the edge of the model in a way that could not be represented in the composite shell model. Also, the coating distorts considerably in the vertical direction while the substrate remains essentially undeformed mechanically. The dimension of 37.8 mm gives some perspective of the scale of

the model and the localization of the deformation, keeping in mind that the thickness of the polymer is 0.02 mm. It is important to note that the maximum tensile principle strain in Figure 7 is located in the middle of the polymer layer, away from either interface. Under appropriate conditions, failure could occur within a material layer rather than at an interface, as assumed in this study.

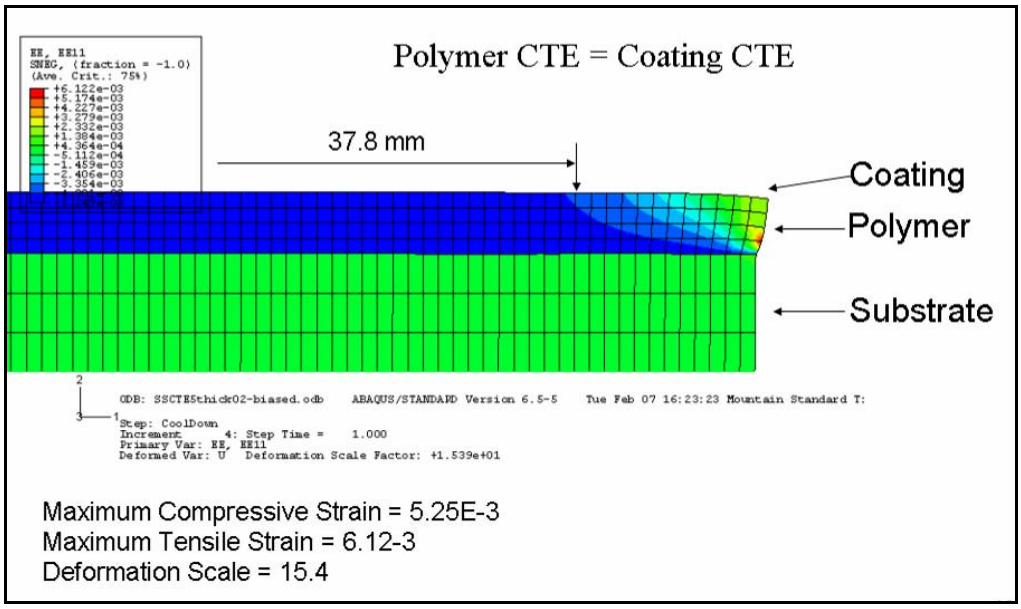


Figure 7: Deformed hybrid model showing elastic strain in the radial direction.

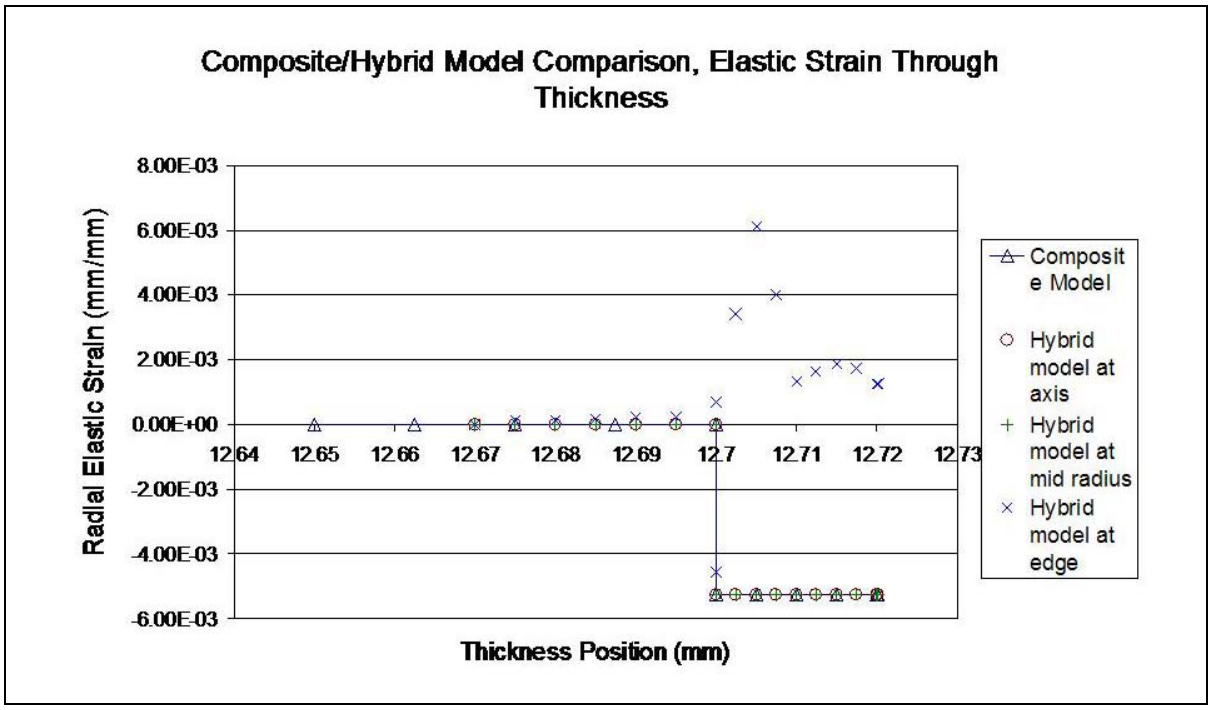


Figure 8. Comparison of composite shell and hybrid models. In this case, the polymer CTE is equal to the coating CTE for both models.

The composite shell and hybrid models correlate very well with each other. The mechanical strain magnitudes in all layers in both models are the same except at the outer edge. The strain calculated using the hybrid model remains constant throughout the radius, acting as predicted by the composite shell model, except at the outer boundary of the model. The magnitude of the mechanical strain calculated at the edge of the hybrid model varies widely as a result of the free material boundaries, as described above and displayed in Figure 8.

The strain difference between layers was also investigated with the hybrid model. A characteristic curve of mechanical strain in the radial direction vs. radius for the polymer and coating is shown below in Figure 9. Although the strain varies in both layers with respect to the radius, the difference between the layers is constant with respect to the radius. This

means that the optic could fail as a result of too great of a strain mismatch at the interface or by exceeding the strain limit of one of the materials at some location along the radius. Again, properly tailoring the CTE of the polymer can reduce the mismatch between layers and change the maximum magnitude of the strain in a particular layer.

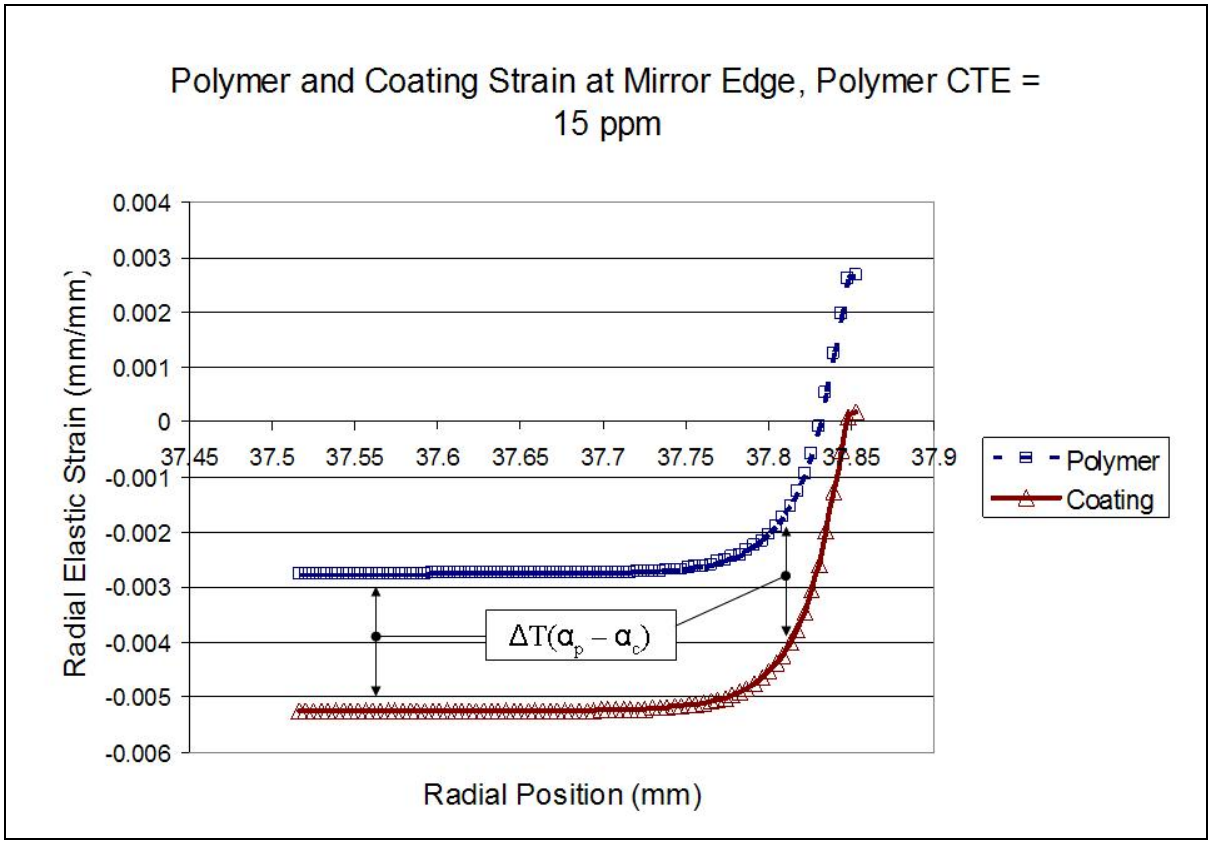


Figure 9. Characteristic strain mismatch between layers. Though the magnitude of strain changes with respect to the radius, the strain mismatch between the layers remains constant.

Aside from constructing an optic that has structural integrity under operating conditions, it is also necessary to predict how the addition of the polymer layer and the alteration of the polymer CTE affect the surface figure of the optic. Without the polymer layer, the mirror experiences a bimetallic bending effect as a result of the difference between

coating and substrate CTE. In Figure 10 below, the relative surface figure deformation of a coating and substrate only is compared to the deformed surface of the coating and substrate separated by polymer layers of different CTE.

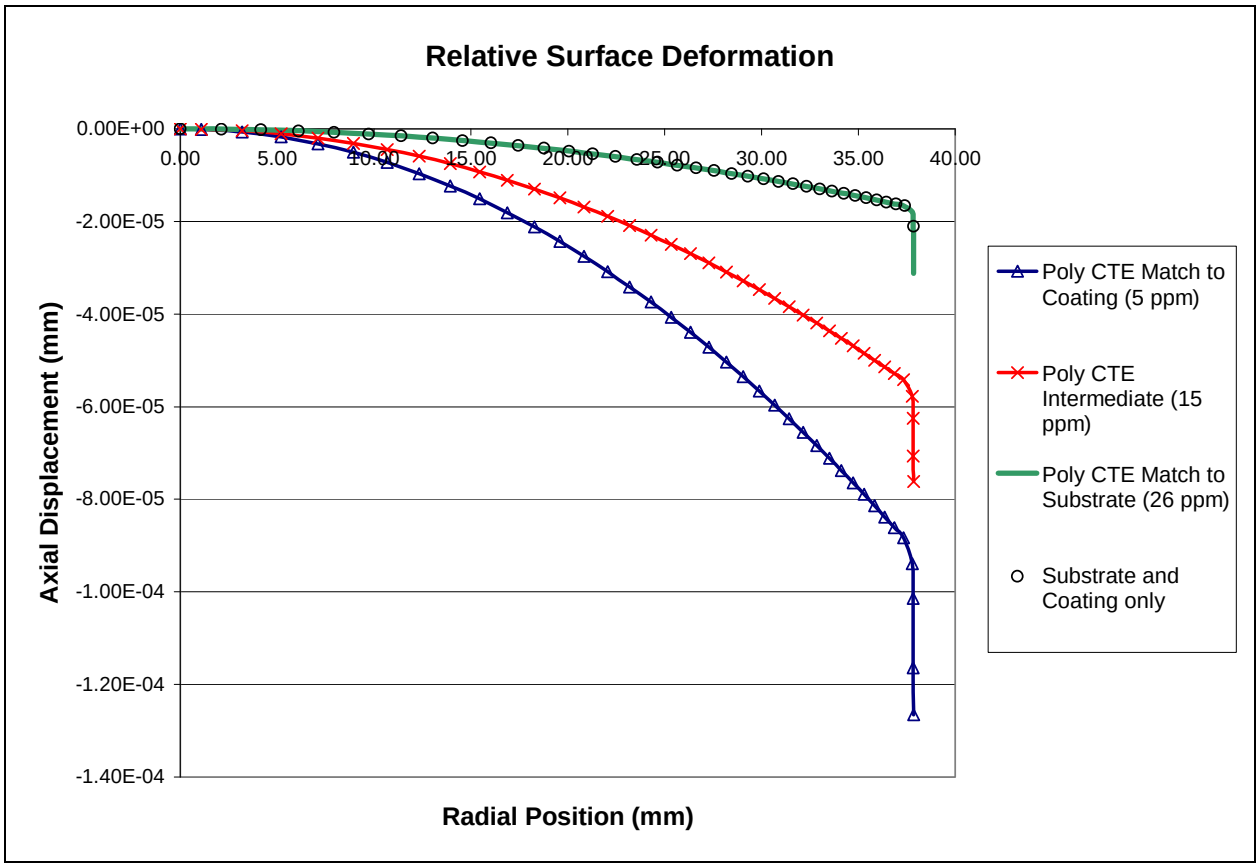


Figure 10. Relative surface figure deformation. When the polymer CTE closely matches the substrate CTE, bending is minimized and has the same curvature as if the polymer layer was absent. However, the greatest strain mismatch occurs between the coating and polymer under this condition. When the CTE of the polymer layer equals the coating CTE, the bending increases, but the strain mismatch between the coating and polymer is zero.

As the CTE of the polymer approaches the CTE of the substrate, the surface deformation is reduced and the flatter the surface remains. Unfortunately this displacement minimization occurs when the thermal strain mismatch between the coating and polymer is

the greatest, but if the polymer has the strength and flexibility to absorb the mismatch, then the mirror is unlikely to fail. This means that the polymer must be tailored to best distribute the strain mismatch as well as maintain the surface deformation within allowable limits. Though not included the figure, realize that the body of the mirror contracts in the focal direction as well as the radial direction. This causes a "piston" shift on the surface of the mirror in addition to the bending. As the CTE of the materials increase, the piston shift increases as well.

RMS was calculated using Equations 2-4 below. Left- and right-hand RMS values were calculated using a Reimann sum (see Equation 3). The right-hand RMS was calculated similarly to the left-hand RMS. Figure 11 shows the two locations for the reference surface, at the highest point on the surface and at the average height of the surface. RMS values for three conditions are tabulated in Table 2 in angstroms. The two locations for the reference plane are for comparison purposes only, depending on where the desired reference plane actually exists.

$$RMS = \frac{1}{2} * \left( RMS_R - RMS_L \right) \tag{2}$$

$$RMS_L = \sqrt{\frac{\sum_{i=2}^{N} \left[ \left( f(x_i) - f(x_{i-1}) \right)^2 * \left( x_i - x_{i-1} \right) \right]}{N * \sum_{i=2}^{N} \left( x_i - x_{i-1} \right)}} \tag{3}$$

$$f(x) = axial\_displacement - reference\_plane \tag{4}$$

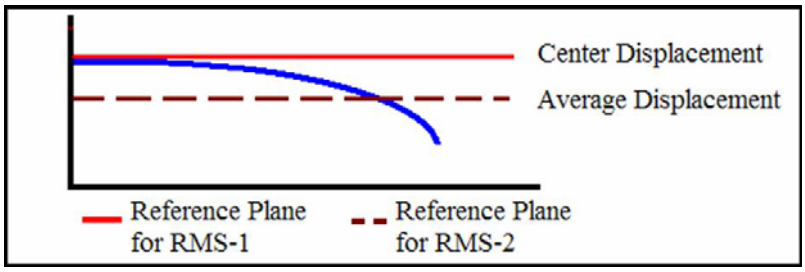


Figure 11. Reference planes for RMS calculations. RMS-1 was calculated by using the deformed location of the center of the mirror (resulting from piston shift) as the axial reference location. RMS-2 was calculated using the average of the deformed axial position as the reference position.

Table 2. Surface RMS for different polymer CTEs. RMS-1 and -2 are reported in angstroms and are calculated according to Equations 2-4.

| Mirror Configuration | RMS-1 (A) | RMS-2 (A) |
|---|---|---|
| Polymer CTE = Substrate CTE (26 ppm*$^{o}C^{-1}$) | 1.29 | 0.8 |
| Coating CTE < Polymer CTE < Substrate CTE (15 ppm*$^{o}C^{-1}$) | 4.22 | 2.82 |
| Polymer CTE = Coating CTE (5 ppm*$^{o}C^{-1}$) | 6.89 | 4.60 |

Because it was desirable to use this technology on different sizes of mirrors, a parametric study of how radius size affects surface deformation and strain magnitude was performed for a half size model and a double size model and compared to the regular size model. The surface deformation for each of these models is shown in Figure 12. These models demonstrate that maximum deflection does not scale linearly with the radius but as

the square of the radius. The curvature of the models is identical, independent of maximum radius.

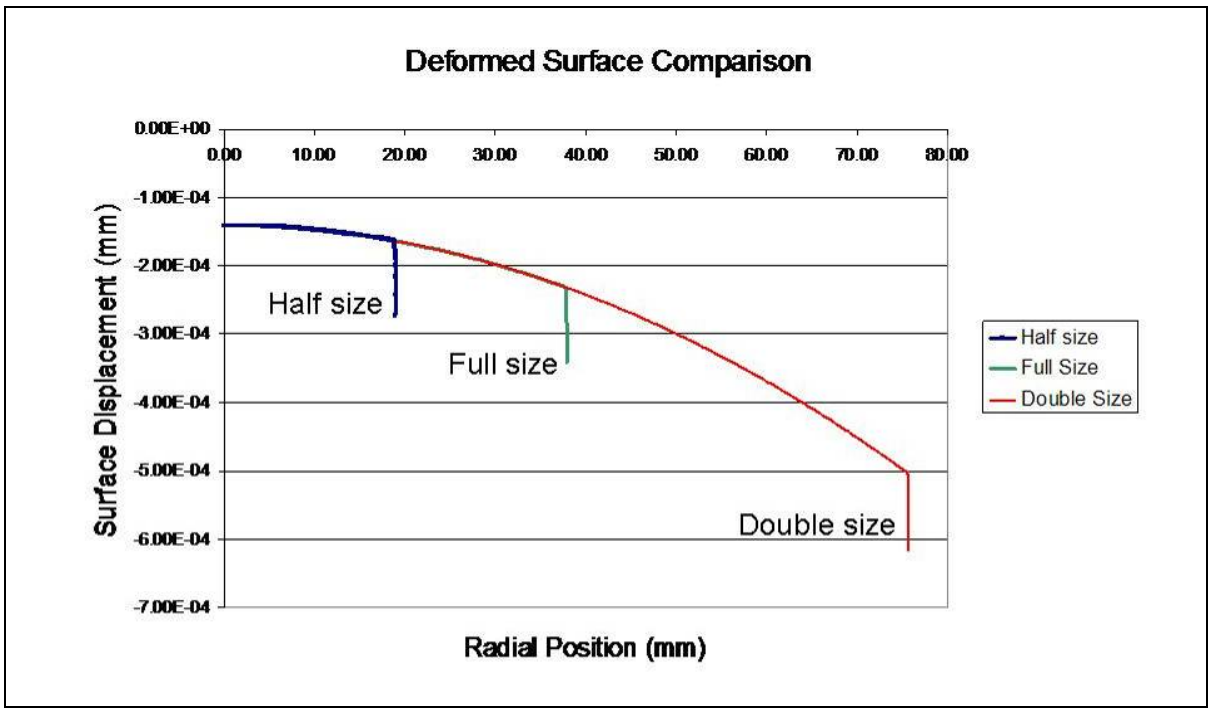


Figure 12: Deformed surface for different radii. Despite the changes in radius, the curvature remains the same. However, the magnitude of bending does not scale. The displacement at a radial position of 0.0 mm is a result of piston shift in the coating layer, polymer layer and first 0.03 mm of substrate.

This deflection behavior corresponds to the bending of a bilayer beams and plates subjected to cooling or heating. For example, for a bilayer beam subjected to a thermal gradient, the curvature of a beam is given by Equation 5, where $M_{Ty}$ and $M_{Tz}$ are area integrals for the thermal moments in the beam due to thermal gradients in the y and z directions, respectively. Integrals for the thermal moments are given in Equations 6 and 7. Curvature is a function of the moment at some position along the beam. The curvature, in this case, is caused by thermal moments, resulting from mismatched CTEs, acting through

the thickness. Since the CTE mismatch is the same along the beam, moments are equivalent as well and so is the curvature. Therefore, curvature is independent of position along the length direction, x. E is a material property, while $I_y$, $I_z$, and $I_{yz}$ are geometric properties of the beam at some position along the length of the beam. T is the temperature as a function of y and z at some point along the length of the beam [Boley and Weiner, 1988].

$$\frac{d^2w}{dx^2} = \frac{-1}{E} * \frac{I_y * M_{Tz} - I_{yz} * M_{Ty}}{I_y * I_z - I_{yz}^2} \tag{5}$$

$$M_{Ty} = \int (a * E * T * z) dA \tag{6}$$

$$M_{Tz} = \int (a * E * T * y) dA \tag{7}$$

The maximum strain magnitude in the polymer with respect to mirror diameter is compared in Table 3. As with curvature, both the maximum principle strain and the maximum shear strain are essentially constant with respect to changes in mirror diameter. Maximum principle strain is constant because it is a function only of the thermal strain mismatch. Shear strain is a function of both the strain mismatch and polymer thickness. Differences in the strain magnitudes can be attributed to slight differences in the mesh density between models.

Table 3. Comparison of maximum elastic strain magnitude in the polymer layer as the mirror diameter changes.

| Model | Max. Principle Strain | Max Shear Strain (1-2 plane) |
|---|---|---|
| Half size mirror | 0.0122 | 0.0338 |
| Full size mirror | 0.0121 | 0.0338 |
| Double size mirror | 0.0123 | 0.0309 |

Intrinsic stress or strain resulting from the coating process can also cause warpage and delamination of an optic. The magnitude of intrinsic stress or strain left in a coating is a function of the temperature, process, thickness, and material used to create the coating [Ohring, 2002]. An intrinsic stress of plus or minus 1.0 GPa is not uncommon. A 1 GPa intrinsic stress was applied to the hybrid model, which then was cooled 250 ˚C as was done with the other models. No matter whether the polymer was present or not, nor what CTE was applied to the polymer, intrinsic stresses of this magnitude dominate the strain mismatches by an order of magnitude, as shown in Figure 13. In Figure 14, the deformed shapes and corresponding mechanical strain in the radial direction, resulting from 1 GPa biaxial compressive and tensile intrinsic stresses and cooling of minus 250 ˚C, are shown. In these cases, the CTE of the polymer is 5 ppm.

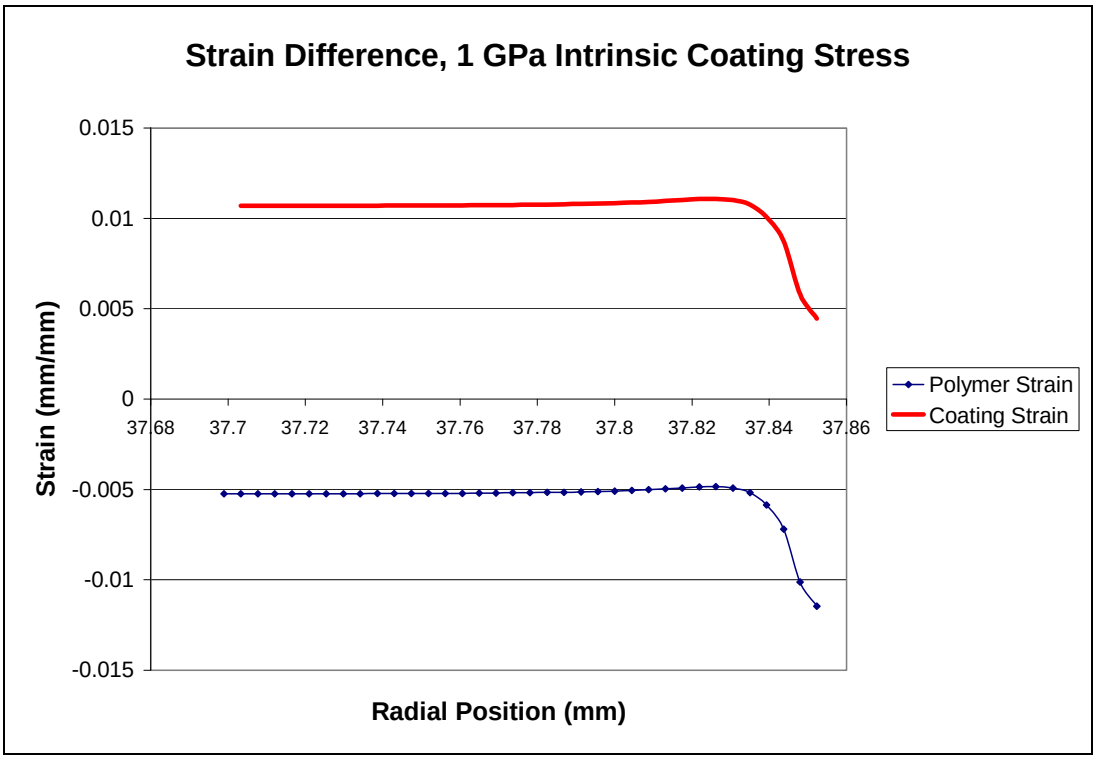


Figure 13. Strain difference between the coating and polymer with a polymer CTE equal to 5 ppm and a 1 GPa biaxial, intrinsic coating stress. Without the intrinsic stress, under this condition there would be no strain mismatch between the coating and polymer. The maximum strain mismatch due to thermal loading is 5.25e-3, an order of magnitude smaller that what is seen here.

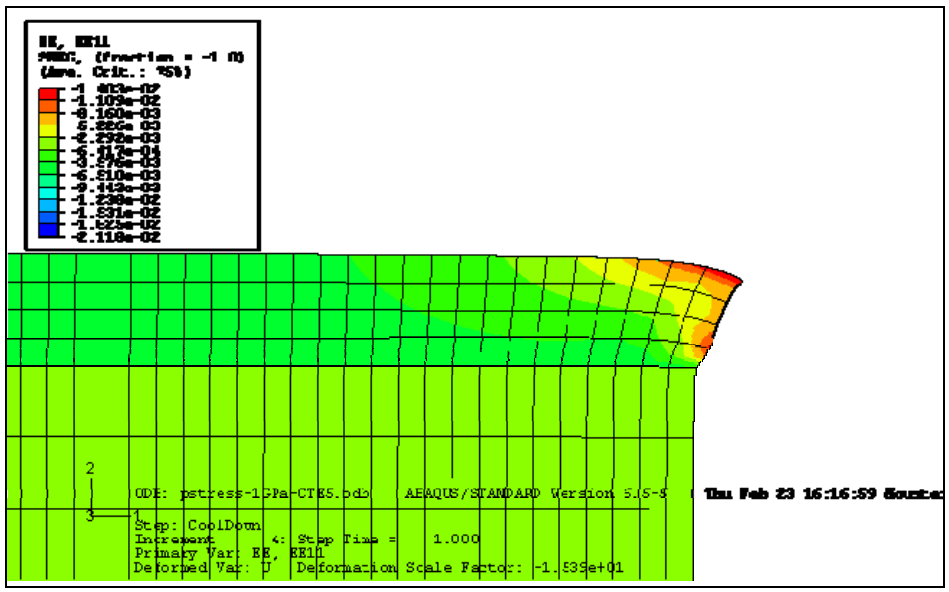


a.

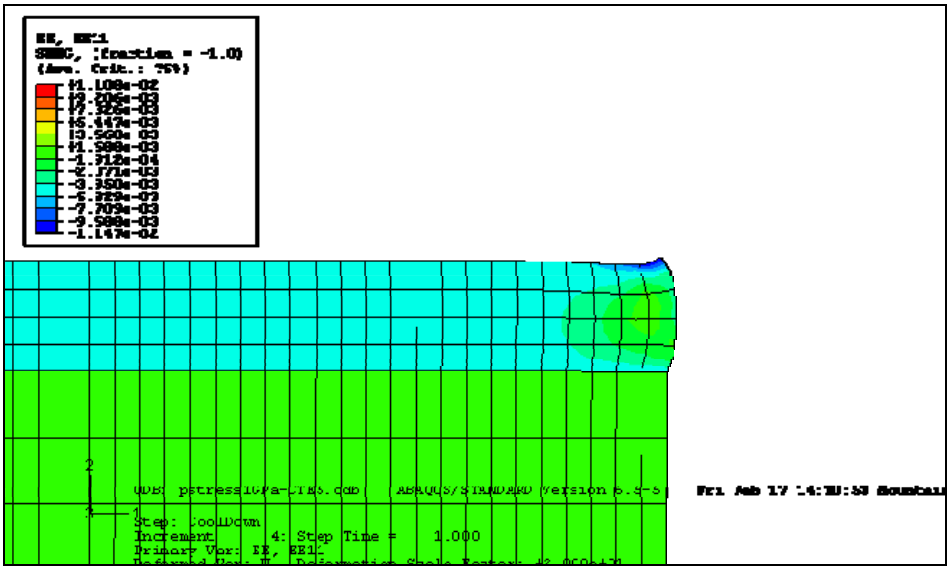


b.

Figure 14. The hybrid model deformed as a result of cryogenic cooling and: a. a 1 GPa intrinsic, biaxial compressive stress in the coating, and b. a 1 GPa intrinsic, biaxial tensile stress in the coating.

## 3-D Hybrid Model

A 3-D model was constructed with materials and dimensions identical to the hybrid model to compare deformations due to gravity with and without the polymer layer. This model was constructed to demonstrate the process for finding gravitational deformations in a hybrid model and not to determine absolute RMS deflection values. Values for RMS deflection for a particular optic are strongly dependent on geometry and boundary conditions, both of which were unspecified for this study. The substrate layer and polymer layer were constructed completely with continuum elements, 19168 and 5504, elements respectively. The coating layer was constructed with 5504 shell elements. The substrate was pinned along the back edge, away from the coatings. An acceleration of -9.81 $m/s^2$ was applied to the model in the axial direction and parallel to the surface to simulate loadings due to gravity in two orientations. Tie constraints were used to join the layers together. Images of the deformed coating layer under the two loading conditions with the polymer layer present are shown in Figure 15, with maximum deflections on the order of +/- 0.5 μm. The deformed surfaces without polymer layers are very similar. The peculiar deformation fringes are print-through of the coarser-meshed substrate nodes on the coating. Though visible, the contribution to RMS deflection is assumed minimal.

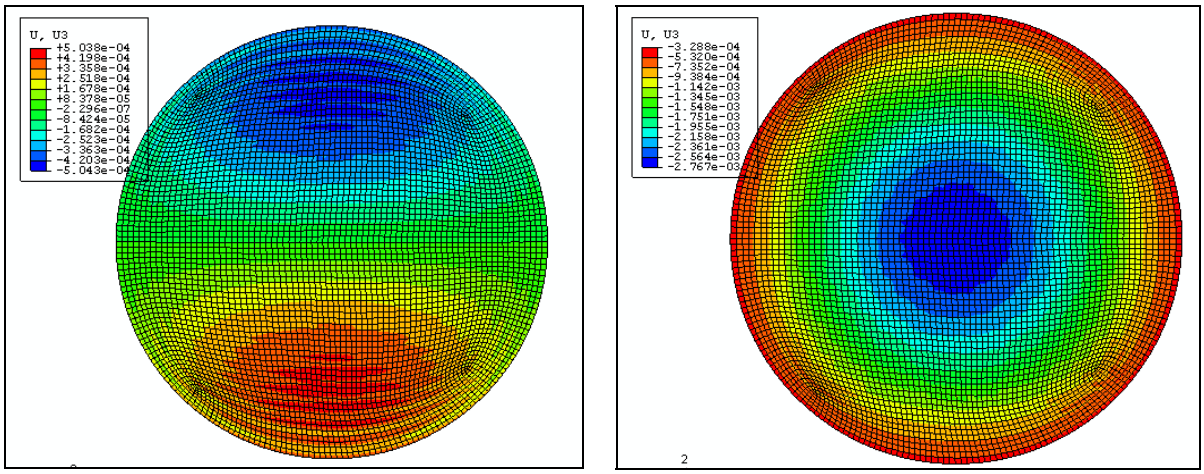


a. b.

Figure 15. Deformed coating surface of models including the polymer layer due to gravity loading in directions: a. parallel to the surface, and a. in the axial direction.

The displacement of the coating nodes in the axial direction were then output to a text file and imported into a spreadsheet. The RMS deflection was then calculated using Equation 8, below, assuming a displacement of zero for the reference plane. This calculation assumes each node represents an equal area across the surface of the model. $U_i$ is the deflection in the axial direction of the ith node from the initial position, N is the number of nodes, A is the total area, and a is the average area per node.

$$RMS = \sqrt{\frac{\sum_{i=1}^{N}\left[\left(u_i^2\right) * a\right]}{N * A}} \tag{8}$$

The RMS deformation for each case is listed below in Table 4. The RMS for the axial loading case is essentially the same whether the polymer layer is present or not. However, it varies slightly for the transverse loading, possibly due to nodal print through.

Therefore, the polymer layer does not contribute negatively to the surface shape of the optic under gravitational loading.

Table 4. RMS surface distortion of coating surface under gravitational loading.

| Loading condition | Parallel gravity load RMS (nm) | Axial gravity load RMS (nm) |
|---|---|---|
| Without polymer layer | 1 | 1 |
| With polymer layer | 0.85 | 0.99 |

## Model Conclusions

Based on the data from the composite shell model and the hybrid model, tuning the CTE of the polymer affects the strain mismatch between the materials and the surface figure of the optic. Smaller values for the polymer CTE, approaching the coating CTE, increase the surface deformation and the strain mismatch at the interface with the substrate but reduce the strain mismatch at the coating interface. Larger values of the polymer CTE, approaching the CTE of the substrate, reduce the surface deformation and strain mismatch at the substrate interface but increase the strain mismatch at the coating interface. Strain mismatches at a particular interface remain constant with respect to radial position, but strain magnitudes within a material layer vary both radially and through the thickness. Deformation caused by CTE mismatches does not scale linearly with respect to changes in radius, but the curvature as a function of radius remains constant. The maximum principle and shear strains within the polymer layers also remain constant. Also, intrinsic stresses and strains can increase strain mismatches significantly, overshadowing the effects of thermal loading.

The 3-D hybrid model shows that the polymer layer does not significantly help or hinder the surface figure distortions due to gravitational loading. Apparently, the distortions are dominated by the substrate. Nothing is gained or lost under these conditions by including the polymer interlayer. Other means of stiffening the mirror against gravity distortions must be implemented if gravitational distortions are an issue.

# 5. DELAMINATION EXPERIMENT

## Purpose and Procedure

An experiment was performed to provide baseline physical data for delamination due to CTE mismatch in coated optics. This data was then used to qualitatively validate a 3D cohesive zone model. The test article was not designed as a service optic, but rather only to study delamination. However, the test article was traceable to the 3-component models described in Section 4.

To construct the samples, materials were chosen according to availability, CTE, and available engineering properties. For the substrates, four 50.8 mm x 5.5mm thick silicon disks and one 60 mm x 12 mm thick silicon disk were donated by Lattice Materials Corporation, Bozeman, Montana. The intermediate polymer layer was simulated with FM 300-2K polymer adhesive, 0.33 mm thick, donated by Cytec Industries, Havre de Grace, Maryland, and the coating was simulated with off-the-shelf heavy duty aluminum foil, 0.025 mm thick.

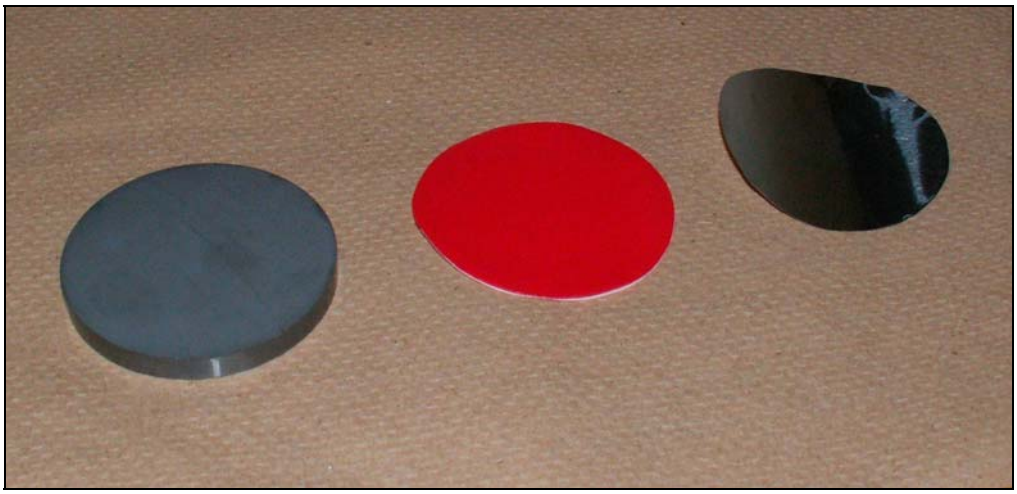

Figure 16. The materials used in the experiment. A 50.8 mm silicon disk is on the left, a circle of FM 300-2K adhesive film is in the middle and a circle of heavy duty aluminum foil is on the right.

The FM 300 polymer is intended for use with aluminum and comes with very specific instructions for surface preparation before use and for proper curing for the best bond strength. Consistency and delamination were of primary importance, the strongest possible bond was not. Moreover, since other materials were used in addition to aluminum, simpler methods of surface preparation and curing were used. Aluminum circles were cut using one of the silicon disks and razor blade. The aluminum and silicon were then rinsed, first with denatured alcohol and then with acetone to remove any oil on the surface. Latex gloves were used during and after rinsing to avoid recontamination. In order to initiate delamination, a strip of 19 mm Teflon thread sealing tape was placed on the disk just before placing the adhesive on the disk to create a crack between the adhesive and silicon approximately 12.7 mm deep as shown in Figure 17.

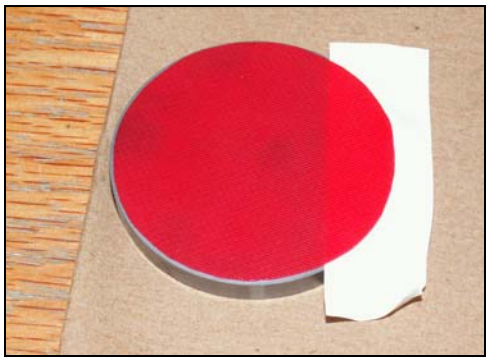

a.

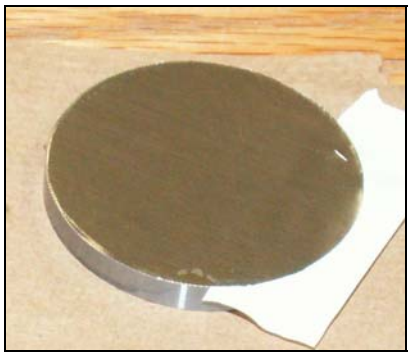

b.

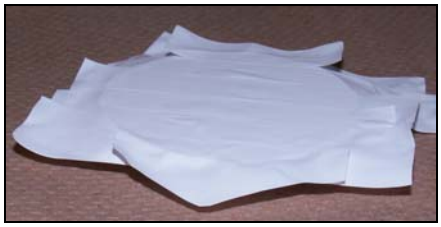

c.

Figure 17. a. Adhesive placed on a silicon disk with Teflon tape used to seed a 12.7 mm crack between the adhesive and the silicon. The adhesive was cut slightly smaller than the disk to minimize adhesive running out over the edge of the disk during curing. b. Aluminum foil placed on the adhesive. c. A double layer of Teflon tape to prevent the adhesive from sticking to the hot plate press during curing.

The aluminum was then carefully placed on top of the adhesive, trying to minimize the amount of creases in the foil as much as possible. An overlapping, double layer of Teflon tape was then placed on top of the foil to prevent any adhesive that leaked from sticking to the curing setup. Because the adhesive is supposed to be cured under a slight pressure, the sample was placed in a hot plate press between two aluminum pucks, as shown in Figure 18.a, and closed until the hot plates just closed on the sample. The sample was heated to approximately 135 ˚C until the adhesive turned from red to orange. As shown in Figure 18.b, if the pressure was too great, much of the adhesive was squeezed out of the sample.

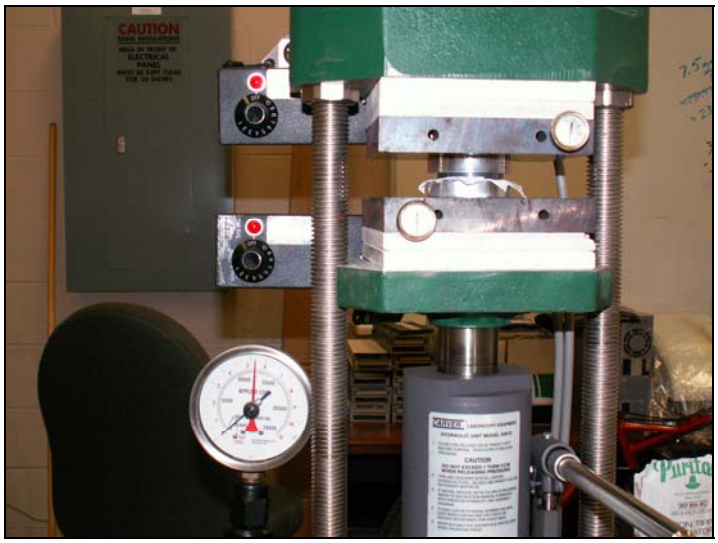


a.

b.

Figure 18. a. The hot plate press with the first sample between two aluminum pucks. This picture is prior to heating. b. Much of the adhesive was squeezed out of the sample, to such a degree that the woven carrier in the adhesive can be seen imprinted in the aluminum. The press is also slightly uneven. The excess adhesive around the crack was broken off before cooling.

Despite the less than satisfactory curing, the sample was cooled by placing it on an aluminum puck partially submerged in liquid nitrogen, with a boiling temperature of approximately minus 190 ˚C. Before cooling, the excess adhesive around the crack was broken off to create a more ideal sample. The sample was cooled for several minutes until a thin layer of frost formed on the sample and the excess adhesive left around the sample broke off the edge, taking some of the silicon with it as shown in Figure 19. Though the foil and adhesive did not peel, the cracking around the edge showed promise.

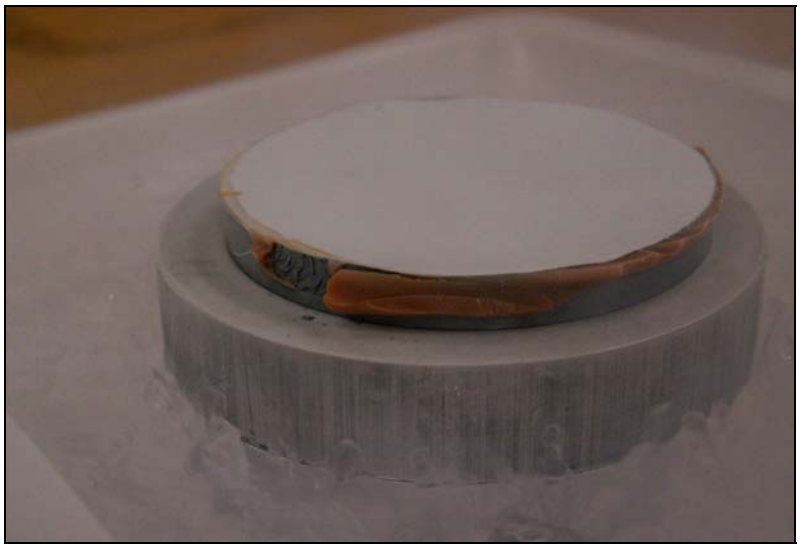

Figure 19. Sample 1 during cooling after some of the adhesive began peeling off of silicon around the edge of the sample.

The second sample was created in the same manner as the first except instead of being pressed between the hot plates, only the bottom hot plate was used to cure the sample and an aluminum puck was used to apply a light pressure on the sample. Also, only half of the sample was covered with aluminum and cracks were seeded on both sides in order to see the effect of bare adhesive on the substrate. Unfortunately, as shown in Figure 20.a, the sample was disturbed midway through cooling and was not as smooth as desired. During cooling however, the sample did peel, as was hoped, along the crack face as well as several other locations as shown in Figure 20. Also, some liquid nitrogen was spilled on top of the sample near the end of the cooling phase, causing some cracking of the foil. Finally, the foil was cut perpendicular to the crack, and the foil and adhesive layers were peeled back to observe a crack approximately 12 mm deep. Failure in this sample and the samples described later all exhibited failure of the substrate material rather than interfacial failure. Material failure such as this must be considered in future work.

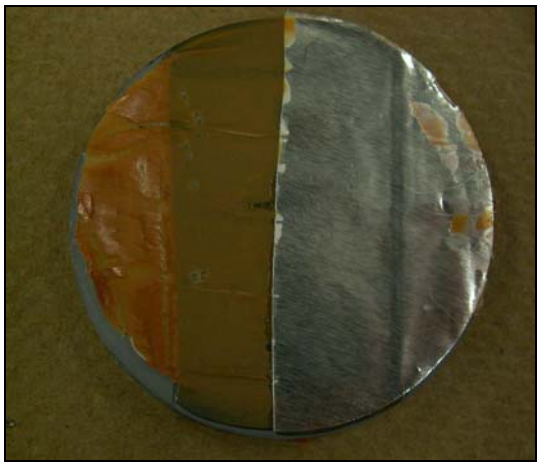

a.

b.

c.

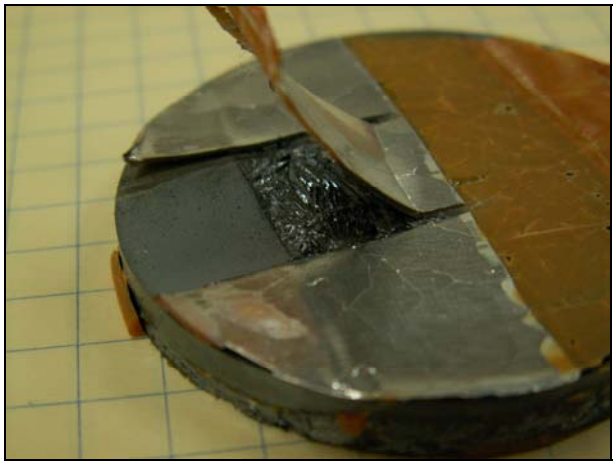

d.

Figure 20. Sample 2. a. The sample after curing. The disturbance while curing mangled the free edge of the bare adhesive and slightly wrinkled the free edge of the aluminum. b. The sample after curing. The aluminum and adhesive layers remain peeled up slightly and a small crack has appeared at the corner of the aluminum. c. A larger crack at the other corner of the aluminum and a good view of the cracking around the edge during the cooling of sample 1. d. The aluminum layer is lifted back revealing that the crack has propagated about 12 mm further into the sample.

The third sample was manufactured identically to the second sample except it was not disturbed during curing and was assembled with a full circle of aluminum foil. This sample was not wrinkled and curing was stopped when the adhesive turned orange. The foil did slip slightly towards the crack side, as seen in Figure 21.a and so was trimmed with a Dremel

tool. During cooling, instead of cracking part way across the sample, the entire adhesive and foil layers popped off completely. Upon further inspection, several defects around the edge contributed to cracking all the way around the sample and complete failure as seen in Figure 21.d. The curvature of the foil and adhesive also indicated some residual stresses from curing.

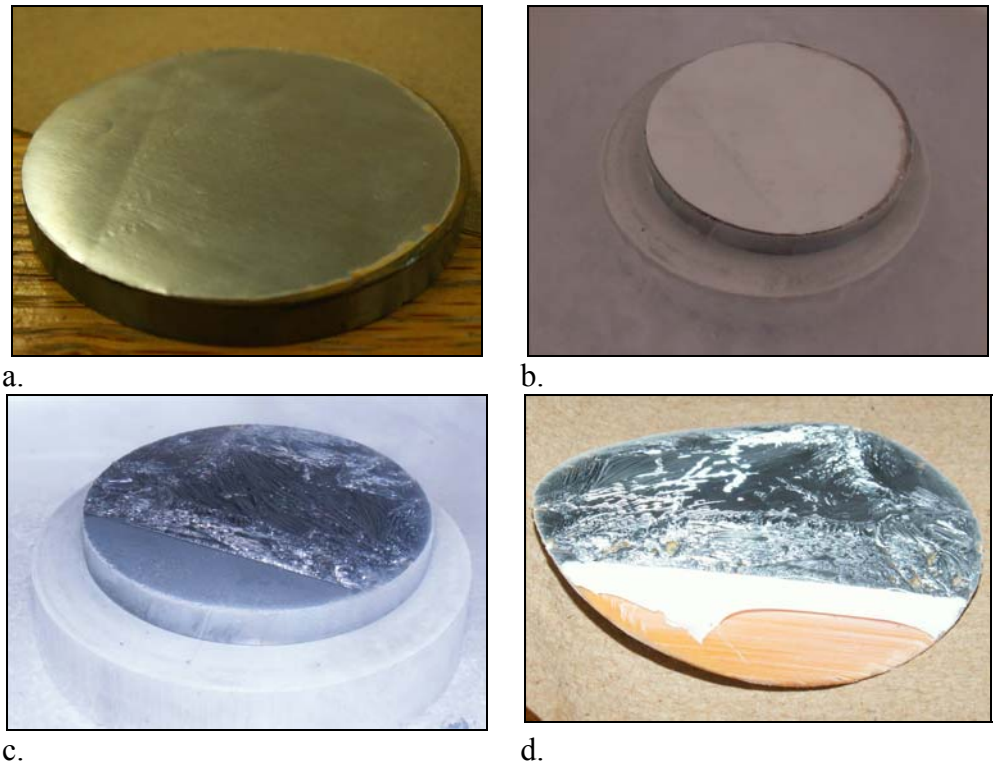

a. b. c. d.

Figure 21. Sample 3. a. During curing the foil slid slightly towards the crack and the excess was trimmed with a Dremel tool. b. Sample 3 during cooling. c. The substrate from sample 3 after the foil and adhesive have popped off. d. The foil and adhesive after they popped off the substrate. The small orange dots in the fracture region are bubbles where the adhesive did not stick to the substrate, promoting the crack to grow. The white region is Teflon tape that was stuck in the crack.

Samples 4, 5 and 6 were assembled at the same time, identically to Sample 3, except Sample 6 was manufactured with the larger silicon puck, as shown in Figure 23. During

curing, the Teflon tape expanded slightly, leaving shallow depressions in the surface. Slight slipping occurred on these samples as well and all were trimmed in the same manner as before.

Figure 22. Samples 4, 5, and 6 during curing.

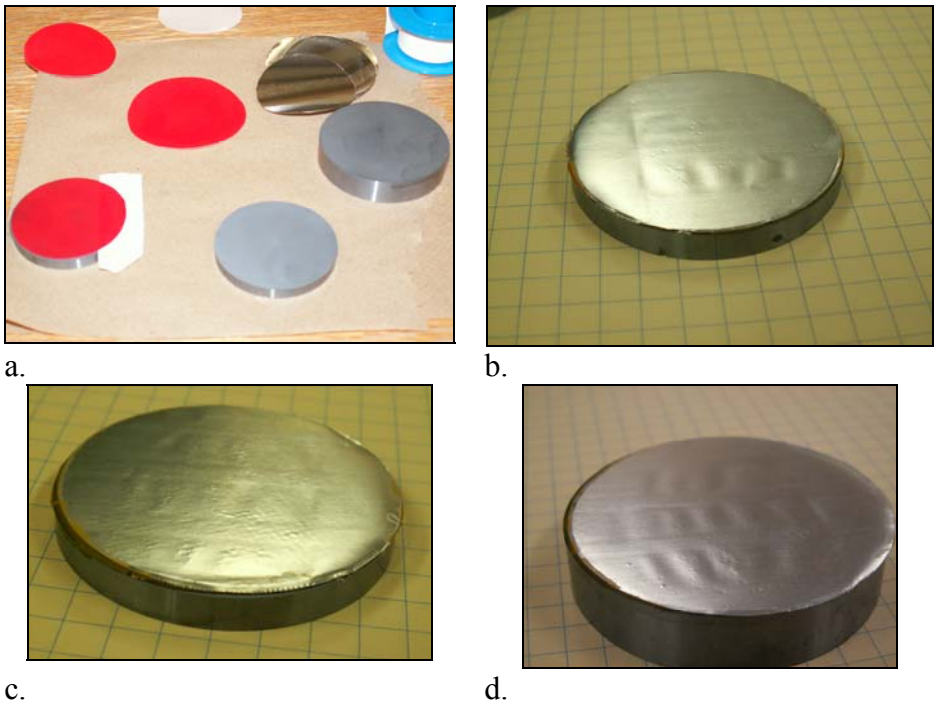

a. b. c. d.

Figure 23. Samples 4, 5, and 6. a. During assembly. b-d. Depressions and slippage in Samples 4, 5, and 6, respectively.

At this point, it was important to know the temperatures that were being reached in the samples. An Agilent 34970A data acquisition and switch unit with a type J thermocouple was used to measure the temperature on the foil surface during cooling of the last three samples. A small ball of DAP™ fun-tak® was used to stick the thermocouple to the foil and insulate it slightly. The fun-tak was chosen over a more traditional glue or adhesive to minimize the contraction effects from cooling a material permanently bonded to the aluminum. It was also easy to remove from the thermocouple once the fun-tak returned to room temperature. The thermocouple was held to the foil until the fun-tack froze. This worked well down to a temperature of approximately minus 120 ˚C, beyond which the fun-tak popped off. At that temperature, some cracking could be heard but no visible cracks were noticed. Based on the rate of cooling that was occurring on the surface of the samples close to minus 120 ˚C, and the fact that the minimum temperature that could be reached was minus 190 ˚C, it was estimated that most of the cracking occurred between the temperatures of minus 130 and 150 ˚C.

Sample 4 was cooled until cracking could be heard from the sample. It was removed from the aluminum puck immediately and warmed to prevent the adhesive from completely popping off again. The foil was cut in a similar manner as was done with Sample 2. After inspection, the only crack could be found at a defect around the edge from the crack and shown in Figure 24.b. This crack was approximately 4 mm deep and 18 mm along the circumference of the sample.

Sample 5 was placed on the aluminum puck with the thermocouple attached as described above and cooled as before. After cooling, the seeded crack face had propagated

an average of 10 mm from its original position. Another crack, approximately 6 mm deep and 32 mm along the circumference also grew, slightly interfering with the seeded crack. One other, very small crack was observed. Sample 6 was cooled using the same process as Sample 5. The seeded crack grew to an average of 3 mm along with several other very shallow areas of delamination.

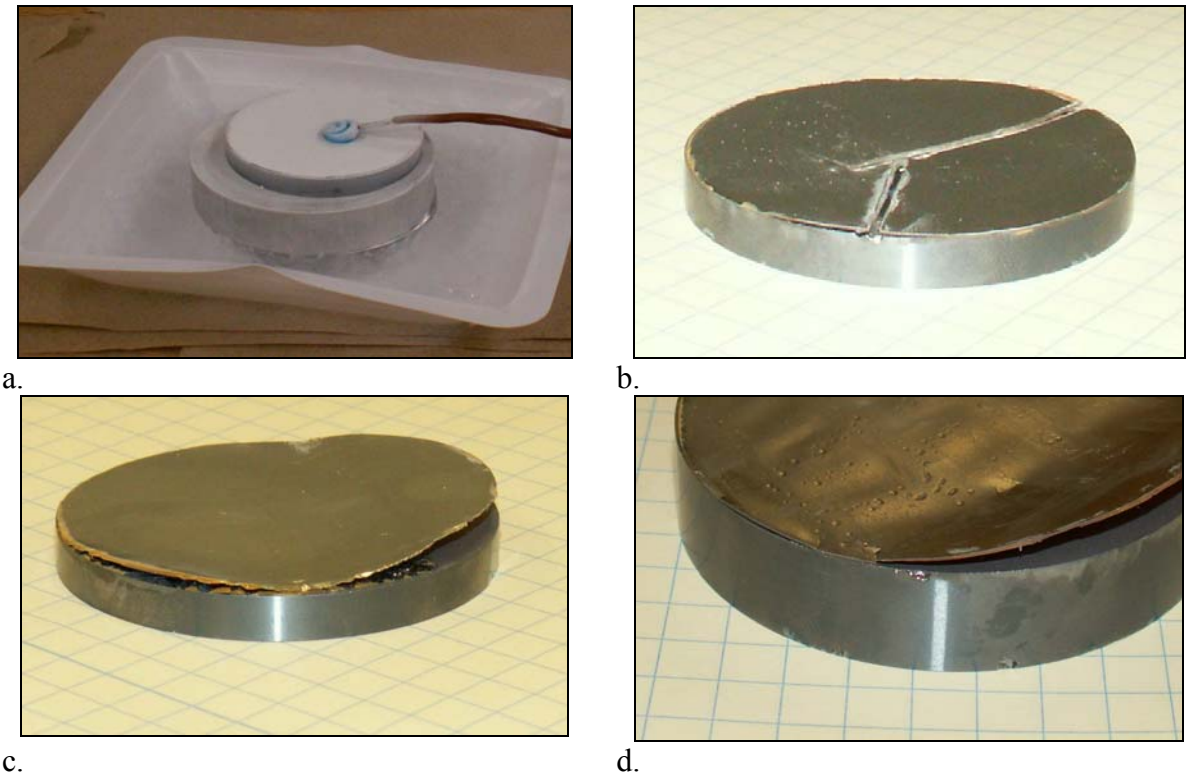

a. b. c. d.

Figure 24. a. Sample 4 with thermocouple attached during cooling. b. Crack on the edge of Sample 4 after being cut with a Dremel tool. c. The intersection of the two cracks on Sample 5. The region where the crack was seeded can be seen on the right. d. Sample 6 and the small crack on the edge to the left. A small crack through the adhesive and foil can also be seen at the corner of the seeded crack.

## Experimental Conclusions

Based on the results of this experiment, drastic cracking due to CTE mismatches occurred for these test articles at temperatures between minus 130 and 150 ˚C. The seeded cracks progressed up to 15 mm with the most cracks propagating about 5 to 10 mm. Small defects in the substrate and bubbles in the adhesive also initiated cracks readily. This indicates to the importance of surface preparation and curing procedures used because bubbles and locations of poor adhesion are likely to become crack initiators. Due to the brittleness of the materials, particularly the silicon, the onset of cracking was very sudden and progressed very rapidly. This is important to note when modeling damage because this can cause difficulties with model convergence if the model is very sensitive to small changes in loading and geometry. Additionally, it was the silicon material that actually failed, rather than the silicon/adhesive interface. Aluminum is a much more ductile material than silicon and may not crack as the silicon did, but failure within any of the material layers in addition to failures at material interfaces should be considered as possible locations for the onset of delamination.

# 6. COHESIVE ZONE FINITE ELEMENT MODELS

Two 3-D cohesive zone models were used to match experimental results and verify the cohesive zone modeling approach used to predict delamination. An axisymmetric model, identical in geometry and material properties to the earlier hybrid model, was used to further predict the onset delamination for a coated mirror with a polymer interlayer. Two zero-thickness cohesive zones with identical material definitions were inserted at the coating/polymer interface and the polymer/substrate interface.

## Three-Dimensional Cohesive Zone Models

This model was created to demonstrate the feasibility of using cohesive zone modeling techniques to accurately predict the interfacial delamination of multilayered mirrors. A full cohesive zone model was created along with a quarter-size model. The full model was used to show correlation between it and the more efficient quarter-sized model, which used two boundaries of symmetry as shown in Figure 25. The quarter-size model was then used to correlate delamination initiation in the model with the delamination seen in the experiment. These three-dimensional cohesive zone models were created using continuum and shell elements with temperature degrees of freedom to represent materials used in the experiment. Cohesive elements were inserted between the material layers to represent adhesive bonds.

In the model there are three material layers: the substrate, the adhesive, and a foil coating. For computational efficiency, the substrate layer is comprised of a continuum layer

0.5 mm thick and a shell layer 5.0 mm thick for a total of 5.5 mm. The thickness of the adhesive and foil layers and their material properties are included in Table 5. On either side of the adhesive layer are zero-thickness cohesive layers defined in terms of traction and separation stiffnesses. The cohesive layers represent the bond between the foil and the adhesive and the bond between the adhesive and the substrate. Each cohesive layer has its own material definition because the performance of the adhesive is dependent on the adhered material and the surface preparation of the adherends before adhesion. The assigned properties of the cohesive layers are also presented in Table 5. For the cohesive zones, $k_{11}$ is the normal separation stiffness and $g_{12}$ and $g_{23}$ are the shear separation stiffnesses.

Table 5. Material properties for the cohesive zone model.

| **Component** | **E** (GPa) | **ν** | **α** ($^oC^{-1}$) | **h** (mm) |
|---|---|---|---|---|
| Foil | 70 | 0.33 | 2.5E-5 | 0.0254 |
| Adhesive | 1.82 | 0.4* | 2.1E-5 | 0.33 |
| Substrate | 112.4 | 0.28 | 2.5E-6 | 5.5 |

| **Cohesive Layers** | $\mathbf{k_{11}}^{\dagger}$ (GPa) | $\mathbf{g_{12}}^{\dagger}$ (GPa) | $\mathbf{g_{23}}^{\dagger}$ (GPa) |
|---|---|---|---|
| Layer 1 | 50 | 100 | 100 |
| Layer 2 | 50 | 70 | 70 |

*Estimated material property. †Material property based on correlation with experimental data.

The diameter of the model is 50.8 mm and a crack was seeded between two of the materials 12.7 mm deep by deleting some of the elements in the cohesive layer between the adhesive and the substrate. The purpose of the crack was to force the material layers to peel apart in a controlled location, causing the cohesive region to fail and allow for correlation with experimental results. The meshes for the full and quarter-sized models are shown below

in Figure 25. The cracked regions are indicated by the arrows. Symmetry boundary conditions were applied to the left and bottom sides of the quarter-sized model as indicated by the dashed lines.

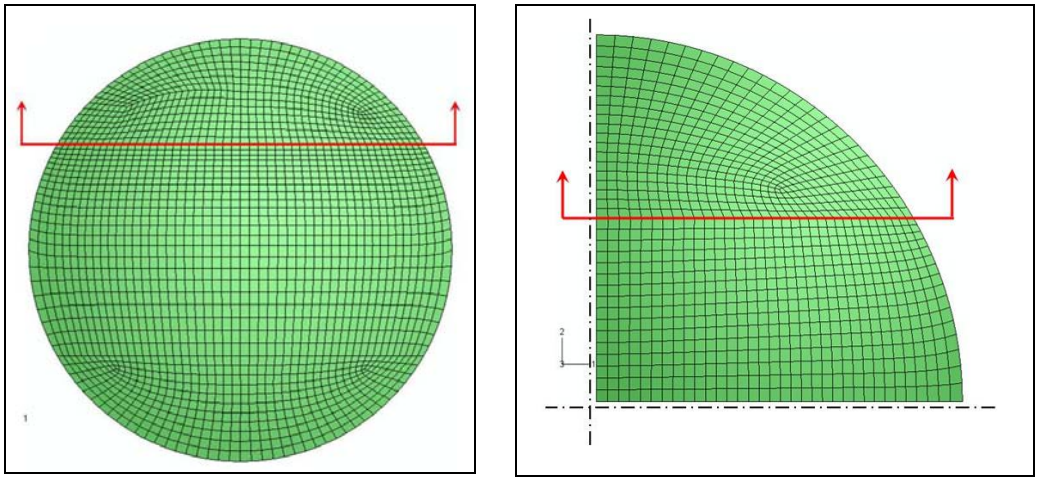

a. b.

Figure 25. a. Front view of the mesh in the full cohesive zone model. b. Front view of the mesh in the quarter-sized cohesive zone model. The full-sized model was fixed at the center and the quarter-sized model was fixed at the lower left corner. The dashed lines represent regions of symmetry boundary conditions.

In the cohesive zones, two variables are used to monitor the condition of the elements. The first is the maximum strain variable, which calculates percent of the total equivalent strain (a function of normal and shear strains) that is present at a node with respect to the maximum equivalent strain allowed before the onset of damage. A maximum value of 1.0 for the maximum strain variable signals the onset of damage. The other variable is the scalar stiffness degradation variable. After damage begins, this variable increases from zero to one, zero meaning damage has yet to occur and one meaning the element has zero stiffness remaining. The points at which damage begins and at which the element is totally degraded are specified in the cohesive material definition in the model. After initial runs of the

models, it was observed that the cohesive region between the foil and adhesive experienced negligible equivalent strain during the thermal cycle. Therefore, damage initiation and evolution for that layer were removed from the model.

Both models were subjected to a negative 155 ˚C temperature change, under steady state assumptions, representing cooling from room temperature to minus 135 ˚C, as estimated from the experiment. The maximum strain variable along the crack face, between the adhesive and substrate, from the midpoint of the crack to the edge of the crack is plotted in Figure 27 for both models. The slight variations between the models are a result of the differences made by the symmetry boundary conditions and slight differences in the mesh. However, the results are similar enough that only the quarter-model was used to correlate with the experimental results.

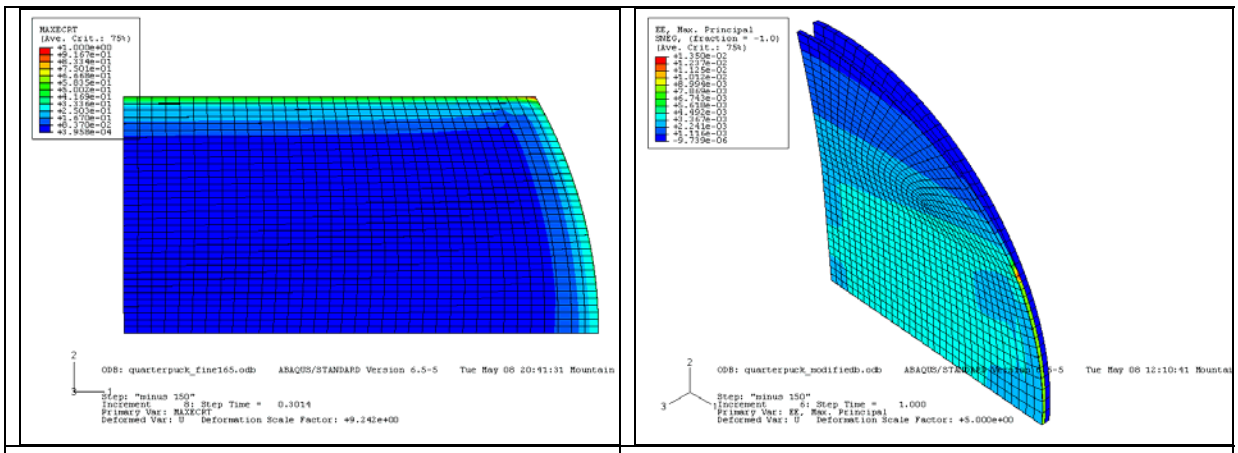

a. b.

Figure 26. Deformed 3-D cohesive zone models. a. The maximum strain variable in the cracked region. The singularity is in the upper left corner. b. Maximum principle strain in the entire quarter model.

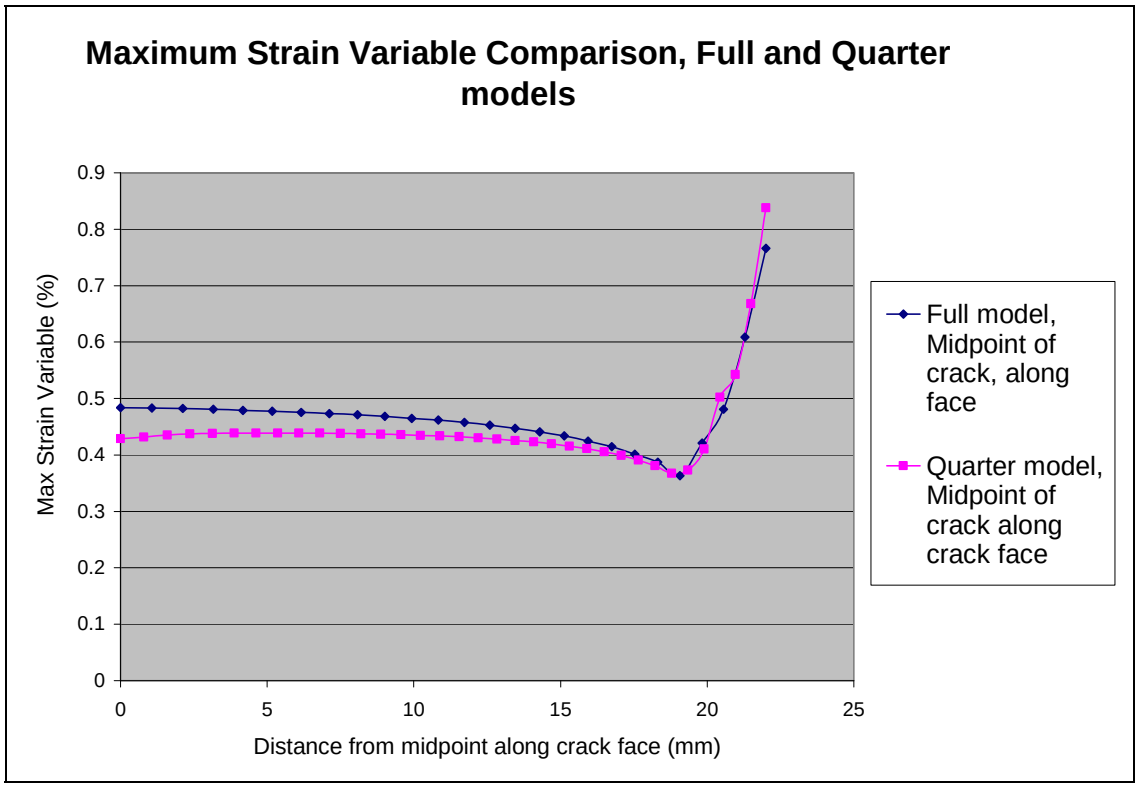


Figure 27. Maximum strain variable comparison between the full and quarter-sized models along the crack face, from the midpoint of the crack to the corner of the crack. By increasing the mesh density in the quarter-model, the damage variable reached a value of 1, or 100% of the allowable equivalent strain before the onset of damage, but convergence after this point was not achieved.

After comparison with the full model, the mesh density of the quarter-sized model was increased to improve solution convergence. After several iterations, the model would converge until a value of 1.0 was reached for maximum strain variable at the corner of the crack. After this value was reached, the model failed to converge and further delamination could not be represented. It was concluded that the corner of the crack created a singularity point and only modification of the geometry of the cracked layer or switching to a dynamic analysis may alleviate the singularity.

The stiffnesses of the cohesive zones were varied along with the maximum allowable equivalent strain to initiate cracking at approximately minus 130 ˚C, the estimated

temperature that cracking began in the experiment. The values of the traction stiffnesses that correlated with the experimental data are listed in Table 6 and the distribution of the maximum strain variable is displayed in Figure 4. The singularity can be seen in the outer corner of the model. Because of the singularity, magnitudes of the maximum strain variable may not be accurate. However, the regions where the maximum strain variable is highest, other than the singularity, appear to correlate well for delamination to initiate at minus 130 ˚C in regions where the cracking was observed in the experimental samples.

Table 6. Cohesive layer material properties between the adhesive and substrate, correlated to experiment results at -130 ˚C.

| Adhesive/Substrate Cohesive layer | $k_{11}$ (GPa) | $g_{12}$ (GPa) | $g_{23}$ (GPa) |
|---|---|---|---|
| Traction Stiffness at damage initiation | 50 | 70 | 70 |

| | $\varepsilon_{11}$ | $\varepsilon_{12}$ | $\varepsilon_{23}$ |
|---|---|---|---|
| Damage Initiation Strains | 6e-4 | 2.75e-4 | 2.75e-4 |

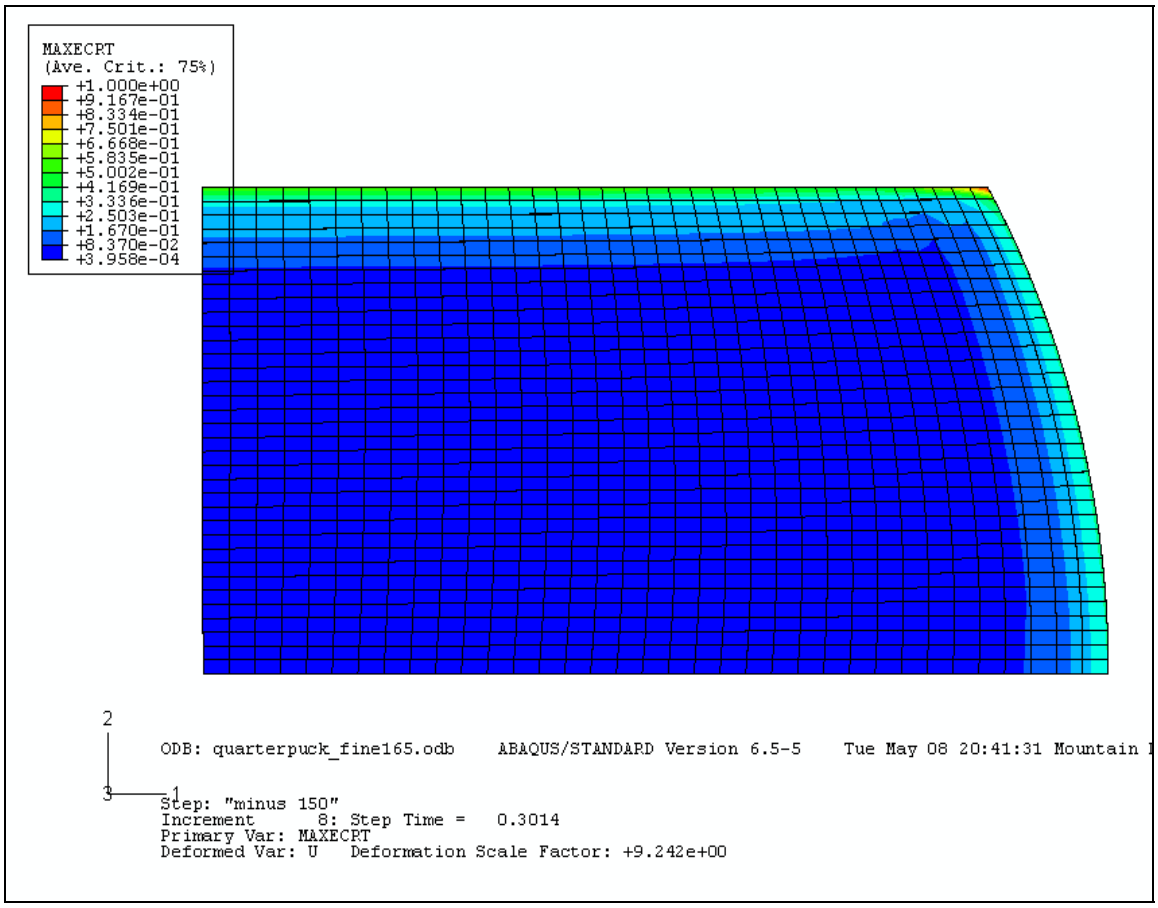


Figure 28. Maximum strain variable in the quarter-sized model. Approximate temperature at this point was minus 115 ˚C.

## Hybrid Cohesive Zone Models

This model was constructed in a fashion similar to the hybrid model, except two cohesive zones were added between the polymer and substrate continuum layers and between the coating shell and polymer continuum layers. Material properties and dimensions for the coating, polymer, and substrate are the same as in the first hybrid model. The model was cooled as before, with steady state assumptions, and the normalized temperature at the onset of delamination was recorded. A schematic of the assembly of the model is shown in Figure

29 and cohesive zone properties are listed in Table 7. These properties were chosen so that delamination was initiated for all four of the following conditions:

1. Polymer layer is not present
2. Polymer CTE = 5 ppm.
3. Polymer CTE = 15 ppm.
4. Polymer CTE = 25 ppm.

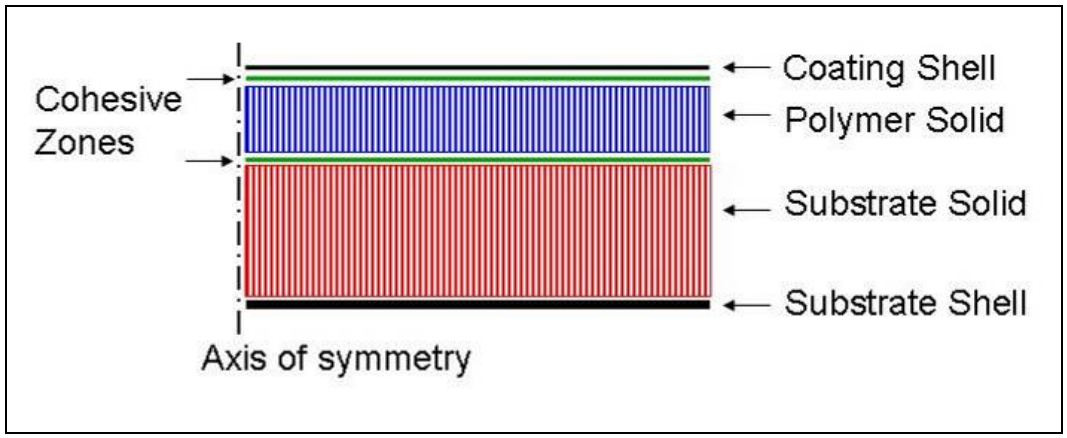


Figure 29. Assembly of hybrid cohesive zone model.

Table 7. Material properties for cohesive zones in the hybrid cohesive zone model.

| | $k_{11}$ (GPa) | $g_{12}$ (GPa) | $g_{23}$ (GPa) |
|---|---|---|---|
| Traction Stiffness | 30 | 15 | 15 |

| | $\varepsilon_{11}$ | $\varepsilon_{12}$ | $\varepsilon_{23}$ |
|---|---|---|---|
| Damage Initiation Strains | 1.0e-4 | 0.5e-4 | 0.5e-4 |

A parametric comparison was made between the temperature at which delamination begins and the CTE of the polymer. Delamination was assumed to begin when the maximum strain variable reached a value of 1.0 at either cohesive zone. For the case with no polymer interlayer, the material properties of the polymer were changed to those of the substrate and

the thickness of the substrate shell was changed accordingly. The normalized results are displayed below in Table 8. A relative temperature value of -1.0 was chosen for the temperature at which delamination begins for the case with the coating and substrate only. As can be seen, tuning the CTE of the polymer to a value below that of the substrate lowers the relative temperature needed for delamination initiation between the polymer and substrate. Under these conditions, not only are the thermal strains of the coating pulling on the substrate interface, but the thermal strains of the polymer are as well, creating additional loading on the interface. However, if the CTE of the polymer is matched to the substrate, the relative temperature to initiate delamination between the polymer and coating is 17 percent below the case without a polymer and there is little loading between the polymer and substrate.

Table 8. Relative temperature marking the onset of delamination at either cohesive zone in the hybrid cohesive zone model and the maximum strain variable at the other cohesive zone.

| Polymer CTE* | Relative Temperature | Damaged Cohesive Zone | Max Strain Variable at other cohesive zone |
|---|---|---|---|
| No Polymer | -1.0 | Coating/Substrate | NA |
| CTE = 5 ppm | -0.39 | Polymer/Substrate | 0.02 |
| CTE = 15 ppm | -0.72 | Polymer/Substrate | 0.3 |
| CTE = 25 ppm | -1.17 | Coating/Polymer | 0.2 |
| CTE = 27 ppm | -1.06 | Coating/Polymer | 0.06 |

*The substrate CTE was set at 25 ppm and the coating CTE was set at 5 ppm.

## Model Conclusions

Using the 3-D cohesive zone models, the onset of delamination can be predicted if appropriate material data is available. By knowing strain limits of the components of the mirrors, and the strengths and load limits of the adhesion between materials, cohesive zones

can be used to predict single cycle failure and perhaps multi-cycle failure of optics during cryogenic cooling. Stress singularities caused by sharp changes in geometry may hinder or prevent model convergence and indicate the onset of delamination prematurely.

The hybrid cohesive zone model further improved the ability to predict mechanical performance of the optic and helped prescribe polymer CTEs for particular material configurations. If the adhesion properties of the polymer to different coatings and substrates are determined, and the mechanical performances of the coatings, polymers and substrates and known, CTE values for the polymer can be optimized very efficiently.

# 7. CONCLUSION

## Conclusions

Including a polymer interlayer with a tuneable CTE shows promise for reducing the chance of delamination and cracking of coated optics used at cryogenic temperatures. Using FEA procedures such as those used in this study, the polymer CTE can be optimized with respect to delamination temperature and surface deformation.

Incorporating combinations of shell and solid elements and composite element definitions are efficient ways to model across optical length scales. This method has been reported before, but not with such complexity. In addition to the shell and solid element combinations, tie constraints, and cohesive elements were also used. Different element types allow for a variety of results to be obtained, loading conditions to be applied, and efficient ways to model complex phenomena without drastic increases in model complexity

Cohesive zones are helpful to model and predict delamination at material interfaces, especially when knowledge of bond properties is available. Since for this study bond characteristics were not available, FEA models were qualitatively validated by experiment.

## Recommendations

To improve the prescription of CTE for polymer interlayers in coated optics, better knowledge of material performance should be obtained. During this study, questions of how material properties such as elastic modulus and strength change as the polymer CTE is tuned

arose several times. Also, CTE, elastic modulus, and ductility are temperature dependent for most materials. This can have a significant effect in thermal analyses, especially when large temperature changes are being considered. Finally, increased knowledge of the adhesive performances of coatings on the polymers and polymers on the substrates would improve the ability to predict failure of optics due to thermal loading.

Modeling can be improved by considering material failure at other locations in addition to the material interfaces. Also, thermal and gravitational loading should be combined to analyze deformed surface figures for models constructed using realistic geometry and boundary conditions.

## Observations

The following observations were made during the experiment and FE analyses conducted during this study.

1. Using shell elements in place of solid elements minimizes mesh size drastically and reduces model run time.
2. Breaking up a stiff material layer with minimal stress and strain gradients into a thin portion of continuum elements and a thick shell is very effective.
3. When using several input files with similar content and lots of iteration, a documented method of organization is essential.
4. Adhesion and material properties for coatings differ greatly with respect to substrate material, surface preparation, and application process. Obtaining

published data is difficult and creating experimental data is difficult with such thin specimens.

5. Crack propagation rate is very sensitive to the material properties defining damage initiation and evolution. Model convergence is very sensitive to crack propagation rate.
6. Small defects in substrates and adhesives readily initiate cracks, especially in brittle materials and at cold temperatures
7. Measuring temperature in an open environment is very difficult when the measured temperature is drastically different than ambient temperature.
8. Adhering sensors, such as thermocouples, for cold temperature tests is challenging.
9. Care must be taken when curing thermoset adhesive like Cytec's FM-300 because it becomes very fluid and sticky at elevated temperatures.

# REFERENCES

ABAQUS Version 6.5 Documentation. ABAQUS Inc. 2004

Boley, Bruno A. & Weiner, Jerome H. Theory of Thermal Stresses. Dover Publications Inc. Mineola, NY. 1988

Chen, Zhong, Brian Cotterell, Wei Wang, Ewald Guenther, and Soo-Jin Chua. "A mechanical assessment of flexible optoelectronic devices." Thin Solid Films. 2001. Vol. 394, pp 202-206

Doyle, Keith B., Victor L. Genberg, Gregory J. Michels. Integrated Optomechanical Analysis. SPIE Press, Bellingham, Washington. 2002

He, Dongming, Charles Zhand, Daniel Chiang, Tieyu Zheng, Alan Lucero, Roger Stage, and Vasu Atluri. "Comparison of thin film cracking and delamination for aluminum and copper silicon interconnects with organic packaging." Electronic Components and Technology Conference, 2005. Proceedings of IEEE, Vol. 1, pp 349-355

Kendrew, Sarah, P. Doel, D. Brooks, C. Dorn, C. Yates, R. M. Dwan, I. Richardson, and G. Evans. "Development of a carbon fiver composite active mirror: design and testing." Optical Engineering. March 2006. Vol. 45

Lowry, H. S., W. H. Goethert, S. L. Steely, W. R. Simpson, D. H. Crider, and M. F. Breeden. "Optical Coating Considerations." Cryogenic Optical Systems and Instruments XI, Proceedings of SPIE, 2005. Vol. 5904

Lowry, H. S., D. H. Crider, W. H. Goethert, W. T. Bertrand, and S. L. Steely. "Scene Projection Developments in the AEDC Space Simulation Chambers." Technologies for Synthetic Enviornments: Hardware-in-the-Loop Testing X. Proceedings of SPIE, 2005. Vol 5785

Meo, M. and E. Thieulot. "Delamination Modeling in a double cantilever beam." Composite Structures. December 2005. Vol. 71, Issue ¾, pp 429-434

Moon, Il Kweon. Optical Performance of Bimetallic Mirrors. Doctoral Thesis, University of Arizona. 2001

Ohring, Milton. Materials Science of Thin Solid Films, 2nd ed. Academic Press, San Francisco, CA. 2002

Soh, Martin T. K., Charles A. Musca, N. Savvides, John M. Dell, and Lorenzo Faraone. "Evaluation of plasma deposited silicon nitride thin films for microsystems technology." Journal of Microelectromechanical Systems. October, 2005. Vol. 14, No. 5, p 971

# APPENDICES

# APPENDIX A

## HYBRID MODEL VERIFICATION

To verify the hybrid models, a simple comparison study was performed by modeling an axisymmetric, bimetallic plate. The plate consisted of a thick layer of aluminum, 2 mm thick by 30 mm in diameter, and a copper coating on top of the aluminum, 0.2 mm thick by 30 mm in diameter. The layers were meshed in three different combinations and deflection at the interface resulting from a minus 100 °C temperature change was plotted. For the first case, both the aluminum and copper layers were meshed with quadratic, axisymmetric solid elements. In the second case, the aluminum was meshed as before, but the copper was meshed with axisymmetric, quadratic shell elements, with the reference plane offset to the negative side. Finally, for the third case, the copper was meshed as in Case 2. The upper half of the aluminum layer, adjacent to the copper, was meshed as in the first two cases. The lower half of the aluminum layer was meshed with axisymmetric, quadratic shell elements with the reference plane offset to the positive side. A schematic of the cases is shown below in Figure A.1.a. The deflections of the three cases are shown in Figure A.1.b. As can be seen, there is almost no difference between the three meshes. In fact, the results are identical to five decimal places and the sixth decimal place varies only by a value of one.

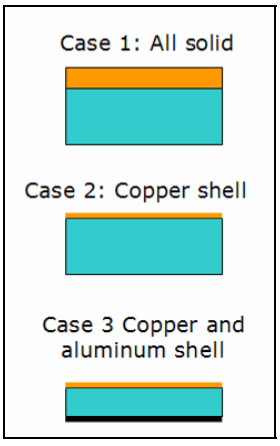


a.

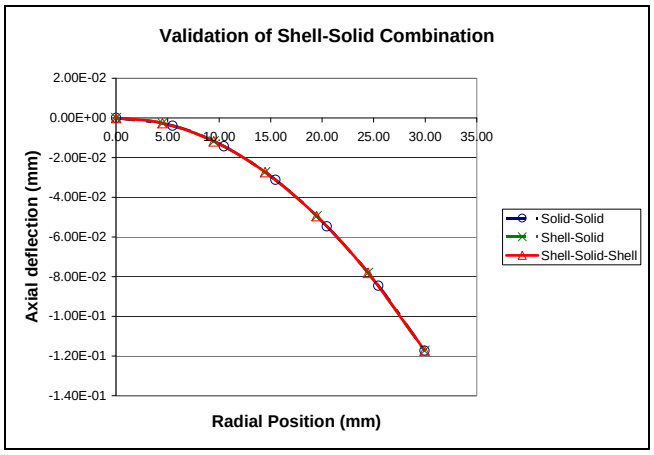


b.

Figure A.1. Cases (a) and deflection data (b) for hybrid model verification.

# APPENDIX B

## COHESIVE ZONE USAGE IN ABAQUS 6.5

Modeling with cohesive zones in ABAQUS CAE 6.5 can be done effectively by following these steps:

1. Create the model geometry, including the cohesive zones. For zero thickness cohesive zones, use an artificial thickness for ease of selection when assigning sections and element types.
2. Create the material definitions in the Property module for all materials in the model. For finite thickness zones, define material properties according to the behavior of the material. Damage initiation and degradation will be assigned later. For zero thickness zones, assign an arbitrary material property for the time being. Material properties will be edited later.
3. Create sections in the Property module for all sections in the model. Create a cohesive section by selecting "Other" in the "Create Section" window. Select the cohesive material that was just created for the cohesive section. Assign the appropriate sections to the appropriate regions and parts in the model.
4. Create the desired steps in the Step module for the analysis.
5. Assign loading, constraints, boundary conditions and other items in the model as usual, keeping in mind that cohesive elements only have displacement degrees of freedom but can be used with heat transfer, coupled temperature-displacement, and coupled thermal-electric analyses.
6. Assign element types to the appropriate regions and parts in the model. Remember that cohesive zones are linear and cannot be meshed adjacent to quadratic elements. Select cohesive elements for cohesive regions and remember to select heat transfer,

coupled temperature-displacement, or coupled thermal-electric elements if needed for other regions. If regions must be removed from the model before submission, an easy way to separate elements is to assign a different element to that region. This separates these elements in the input file for easy deletion.

7. Mesh the regions
8. Create a job in the "Job Manager" window and write and input file.
9. Open the input file using Notepad to edit it. Delete the desired elements if necessary and change the geometry of zero-thickness zones. Then find the "Materials" section.
10. To model damage initiation and degradation in the cohesive zone materials, two keywords must be added to the material definition and the parameters of *Elastic must be changed:

```
*Elastic, Type=Traction
5E4, 10E4, 10E4
*Damage Initiation, Criterion=MaxE
6e-4, 4E-4, 4E-4
*Damage Evolution, Type=Displacement, Softening=linear
3E-4
```

11. The "type" parameter must be changed to "traction" or "coupled traction" and the data line below *Elastic must contain the components of the traction stiffnesses for the cohesive zone if zero thickness zones are used.
12. *Damage Initiation must be added to specify the beginning of damage in the element. This can be specified several ways by changing the parameter "Criterion." Depending on the criterion, the data line below *Damage Initiation must contain the allowable stress, strain, or whatever at the onset of damage.

13. *Damage Evolution must also be added after *Damage Initiation to specify how the stiffness of the element degrades after damage has been initiated. The parameter "type" identifies the variables connected to the evolution of damage and the parameter "Softening" identifies how the damage evolves with changes in the variables connected to damage evolution. The data line below *Damage Evolution is used to specify when damage is complete.
14. Elements are removed from cohesive zones when damage is complete. To control how far damage may progress and to keep totally degraded elements in the model (contrary to default) a section control must be defined.
15. In the part level of the input file (between *Part and *End Part of a particular part), enter the following keyword and parameters:

*Section Controls, Name=Bond-coating-controls, Max degradation=0.99, Element deletion=no

"Name" is the name of the controls used in the section definition. "Max degradation is the maximum percent and element will be allowed to degrade. "Element deletion" gives the option of keeping elements in the model. Other parameters are described in the ABAQUS documentation

16. Find the section definition where controls are desired, probably *Cohesive Section. Add the parameter "controls=name" where "name" is the name of the section controls defined in 15.
17. The cohesive zone definition should be complete. Run the input file and fix any errors if present.

18. More information about cohesive zones can be found in the Keywords Reference manual, Sections 10, 11, and 18 of the ABAQUS Analysis User manual, Sections 12, 21 and 41 of the ABAQUS/CAE User manual, and by searching for “cohesive” in the manual browser.

# APPENDIX C

## ABBREVIATED COMPOSITE SHELL INPUT FILE

```
** PARTS
*Part, name=Part-1
*Node
node number, x coordinate, y coordinate
*Element, type=SAX2T
 element number, first node, middle node, last node
*Nset, nset=_PickedSet2, internal, generate
  first node,  second node,   increment
*Elset, elset=_PickedSet2, internal, generate
  first element,  second element,   increment
*Elset, elset=_PickedSet2, internal, generate
  1,  38,   1
*Shell Section, elset=_PickedSet2, composite
12.2, 5, Aluminum, 0.
0.5, 5, Aluminum, 0.
0.2, 5, CP1, 0.
0.0002, 5, SiO2, 0.
*End Part
** ASSEMBLY
*Assembly, name=Assembly
*Instance, name=Part-1-1, part=Part-1
*End Instance
*Nset, nset=_PickedSet5, internal, instance=Part-1-1, generate
  1,  77,   1
*Elset, elset=_PickedSet5, internal, instance=Part-1-1, generate
  1,  38,   1
*Nset, nset=_PickedSet6, internal, instance=Part-1-1
 1,
*End Assembly
** MATERIALS
*Material, name=Aluminum
*Conductivity
 0.2,
*Elastic
70000., 0.33
*Expansion
 2.6e-05,
*Material, name=CP1
*Conductivity
 0.1,
*Elastic
2170., 0.4
*Expansion
 1.5e-05,
```

```
*Material, name=SiO2
*Conductivity
 0.4,
*Elastic
52100., 0.17
*Expansion
 5e-06,
** BOUNDARY CONDITIONS
** Name: Displacement Type: Displacement/Rotation
*Boundary
_PickedSet6, 1, 1
_PickedSet6, 2, 2
_PickedSet6, 6, 6
** ----------------------------------------------------------------
** STEP: Step-1
*Step, name=Step-1, amplitude=RAMP
*Coupled Temperature-Displacement, creep=none, steady state
0.25, 1., 1e-05, 1.
** BOUNDARY CONDITIONS
** Name: Tempchange Type: Temperature
*Boundary
_PickedSet5, 11, 11, -250.
** OUTPUT REQUESTS
*Restart, write, frequency=0
** FIELD OUTPUT: F-Output-1
*Output, field, variable=PRESELECT
** HISTORY OUTPUT: H-Output-1
*Output, history, variable=PRESELECT
*EL PRINT, POSITION=INTEGRATION POINTS
1, 2, 3, 4, 5
S, EE, THE
*EL PRINT, POSITION=INTEGRATION POINTS
6, 7, 8, 9, 10, 11, 12, 13, 14, 15, 16, 17, 18, 19, 20
s, EE, THE
*End Step
```

# APPENDIX D

## ABBREVIATED HYBRID INPUT FILE

```
** PARTS

*Part, name=Coating
*Node, NSET=NCOATINGSET
*Element, type=SAX2T
*Nset, nset=_PickedSet2, internal, generate
   1,  7001,     1
*Elset, elset=_PickedSet2, internal, generate
   1,  3500,     1
** Region: (Coating:Picked)
*Elset, elset=_PickedSet2, internal, generate
   1,  3500,     1
** Section: Coating
*Shell Section, elset=_PickedSet2, material=Coating, offset=sneg
0.0002, 5
*End Part
*Part, name=Poly-Substrate
*Node
*Element, type=CAX8T
*Elset, elset=_PickedSet4, internal, generate
 14001,  24500,      1
** Region: (Polymer:Picked)
*Elset, elset=_PickedSet3, internal, generate
     1,  14000,      1
** Section: Polymer
*Solid Section, elset=_PickedSet3, material=Polymer
1.,
** Region: (Substrate-Solid:Picked)
*Elset, elset=_PickedSet4, internal, generate
 14001,  24500,      1
** Section: Substrate-Solid
*Solid Section, elset=_PickedSet4, material=Substrate
1.,
*End Part
*Part, name=Substrate-shell
*Node, NSET=NSUBSTRATESET
*Element, type=SAX2T
*Nset, nset=_PickedSet3, internal, generate
   1,  7001,     1
*Elset, elset=_PickedSet3, internal, generate
   1,  3500,     1
** Region: (Substrate-Shell:Picked)
*Elset, elset=_PickedSet3, internal, generate
   1,  3500,     1
```

```
** Section: Substrate-Shell
*Shell Section, elset=_PickedSet3, material=Substrate, offset=spos
12.67, 5
*End Part
**
**
** ASSEMBLY
**
*Assembly, name=Assembly
**
*Instance, name=Poly-Substrate-1, part=Poly-Substrate
*End Instance
**
*Instance, name=Coating-1, part=Coating
        0., 0.0500000000000007,          0.
*End Instance
**
*Instance, name=Substrate-shell-1, part=Substrate-shell
*End Instance
**
*ELSET, ELSET=SUBSTRATESET
SUBSTRATE-SHELL-1._PICKEDSET3
**
*ELSET, ELSET=COATINGSET
COATING-1._PICKEDSET2
*NSET, NSET=NSUBSTRATESET
SUBSTRATE-SHELL-1.NSUBSTRATESET
**
*NSET, NSET=NCOATINGSET
COATING-1.NCOATINGSET
*************************************************************
**
*Nset, nset=_PickedSet14, internal, instance=Poly-Substrate-1
 5,
*Nset, nset=_PickedSet15, internal, instance=Poly-Substrate-1
    1,     4,     5, 10508, 10509, 10510, 10511, 10512, 10513, 10514, 10515, 52514, 59515,
66516, 73517
*Elset, elset=_PickedSet15, internal, instance=Poly-Substrate-1
    1,  3501,  7001, 10501, 17500, 21000, 24500
*Nset, nset=_PickedSet16, internal, instance=Poly-Substrate-1, generate
    1,  80515,      1
*Nset, nset=_PickedSet16, internal, instance=Coating-1, generate
   1,  7001,     1
*Nset, nset=_PickedSet16, internal, instance=Substrate-shell-1, generate
```

```
   1,  7001,     1
*Elset, elset=_PickedSet16, internal, instance=Poly-Substrate-1, generate
     1,  24500,      1
*Elset, elset=_PickedSet16, internal, instance=Coating-1, generate
   1,  3500,     1
*Elset, elset=_PickedSet16, internal, instance=Substrate-shell-1, generate
   1,  3500,     1
*Elset, elset=__PickedSurf10_S3, internal, instance=Poly-Substrate-1, generate
 10501,  14000,      1
*Surface, type=ELEMENT, name=_PickedSurf10, internal
__PickedSurf10_S3, S3
*Elset, elset=__PickedSurf11_SNEG, internal, instance=Coating-1, generate
   1,  3500,     1
*Surface, type=ELEMENT, name=_PickedSurf11, internal
__PickedSurf11_SNEG, SNEG
*Elset, elset=__PickedSurf12_S3, internal, instance=Poly-Substrate-1, generate
 21001,  24500,      1
*Surface, type=ELEMENT, name=_PickedSurf12, internal
__PickedSurf12_S3, S3
*Elset, elset=__PickedSurf13_SPOS, internal, instance=Substrate-shell-1, generate
   1,  3500,     1
*Surface, type=ELEMENT, name=_PickedSurf13, internal
__PickedSurf13_SPOS, SPOS
** Constraint: Constraint-1
*Tie, name=Constraint-1, adjust=yes
_PickedSurf11, _PickedSurf10
** Constraint: Constraint-2
*Tie, name=Constraint-2, adjust=yes
_PickedSurf13, _PickedSurf12
*End Assembly
**
** MATERIALS
**
*Material, name=Coating
*Conductivity
 0.2,
*Elastic
52100., 0.17
*Expansion
 5e-06,
*Material, name=Polymer
*Conductivity
 0.2,
*Elastic
```

```
2170., 0.4
*Expansion
 5e-06,
*Material, name=Substrate
*Conductivity
 0.2,
*Elastic
70000., 0.33
*Expansion
 2.6e-05,
** BOUNDARY CONDITIONS
** Name: BC-1 Type: Displacement/Rotation
*Boundary
_PickedSet14, 1, 1
_PickedSet14, 2, 2
_PickedSet14, 6, 6
** Name: BC-2 Type: Displacement/Rotation
*Boundary
_PickedSet15, 1, 1
_PickedSet15, 6, 6
** ----------------------------------------------------------------
** STEP: CoolDown
*Step, name=CoolDown, amplitude=RAMP
*Coupled Temperature-Displacement, creep=none, steady state
0.2, 1., 1e-05, 1.
** BOUNDARY CONDITIONS
** Name: BC-3 Type: Temperature
*Boundary
_PickedSet16, 11, 11, -250.
** OUTPUT REQUESTS
*Restart, write, frequency=0
** FIELD OUTPUT: F-Output-1
*Output, field, frequency=99999
*Node Output
CF, NT, RF, RFL, U
*Element Output, directions=YES
E, EE, HFL, LE, PS, S, THE, VS
*Contact Output
CDISP, CSTRESS
** HISTORY OUTPUT: H-Output-1
*Output, history, variable=PRESELECT
*EL PRINT, Elset=COATINGSET, POSITION=INTEGRATION POINTS,
FREQUENCY=100
1, 2, 3, 4, 5
```

```
EE, THE
*EL PRINT, Elset=SUBSTRATESET, POSITION=INTEGRATION POINTS,
FREQUENCY=100
1, 2, 3, 4, 5
EE, THE
*NODE PRINT, NSET=NCOATINGSET, FREQUENCY=100
U
*NODE PRINT, NSET=NCOATINGSET, FREQUENCY=100
U
*End Step
```

# APPENDIX E

## ABBREVIATED INPUT FILE WITH COHESIVE ZONE DEFINITION

```
*Part, name=Poly-Substrate
*Node
*Elset, elset=_PickedSet35, internal, generate
 2501,  5000,     1
** Region: (Bond-Substrate:Picked)
*Elset, elset=_PickedSet33, internal, generate
    1,  2500,     1
** Section: Bond-Substrate
*Cohesive Section, elset=_PickedSet33, material=Bond-substrate, response=TRACTION
SEPARATION, controls=Bond-substrate-controls
,
** Region: (Bond-coating:Picked)
*Elset, elset=_PickedSet35, internal, generate
 2501,  5000,     1
** Section: Bond-coating
*Cohesive Section, elset=_PickedSet35, material=Bond-coating, response=TRACTION
SEPARATION, controls=Bond-coating-controls
,
** Region: (Substrate-Solid:Picked)
*Elset, elset=_PickedSet32, internal, generate
  5001,  12500,      1
** Section: Substrate-Solid
*Solid Section, elset=_PickedSet32, material=Substrate
1.,
** Region: (Polymer:Picked)
*Elset, elset=_PickedSet34, internal, generate
 12501,  22500,      1
** Section: Polymer
*Solid Section, elset=_PickedSet34, material=Polymer
1.,
*End Part
*Section Controls, Name=Bond-coating-controls, Max degradation=0.99, Element
deletion=no
*Section Controls, Name=Bond-substrate-controls, Max degradation=0.99, Element
deletion=no
** ASSEMBLY
*Assembly, name=Assembly
*Instance, name=Poly-Substrate-1, part=Poly-Substrate
*End Instance
*Instance, name=Coating-1, part=Coating
         0., 0.05,           0.
*End Instance
*Instance, name=Substrate-shell-1, part=Substrate-shell
*End Instance
```

```
*Nset, nset=_PickedSet14, internal, instance=Poly-Substrate-1
 9,
*Nset, nset=_PickedSet52, internal, instance=Poly-Substrate-1
     2,     3,     5,     8,     9, 10007, 10008, 12510, 12511, 12512
*Elset, elset=_PickedSet52, internal, instance=Poly-Substrate-1
  2500,  2501,  7500, 10000, 12500, 15000, 17500, 20000, 22500
*Nset, nset=_PickedSet53, internal, instance=Poly-Substrate-1
*Nset, nset=_PickedSet53, internal, instance=Coating-1, generate
*Nset, nset=_PickedSet53, internal, instance=Substrate-shell-1, generate
*Elset, elset=_PickedSet53, internal, instance=Poly-Substrate-1, generate
*Elset, elset=_PickedSet53, internal, instance=Coating-1, generate
*Elset, elset=_PickedSet53, internal, instance=Substrate-shell-1, generate
*Elset, elset=__PickedSurf11_SNEG, internal, instance=Coating-1, generate
*Surface, type=ELEMENT, name=_PickedSurf11, internal
__PickedSurf11_SNEG, SNEG
*Elset, elset=__PickedSurf13_SPOS, internal, instance=Substrate-shell-1, generate
*Surface, type=ELEMENT, name=_PickedSurf13, internal
__PickedSurf13_SPOS, SPOS
*Elset, elset=__PickedSurf50_S3, internal, instance=Poly-Substrate-1, generate
*Surface, type=ELEMENT, name=_PickedSurf50, internal
__PickedSurf50_S3, S3
*Elset, elset=__PickedSurf51_S3, internal, instance=Poly-Substrate-1, generate
*Surface, type=ELEMENT, name=_PickedSurf51, internal
__PickedSurf51_S3, S3
** Constraint: Constraint-1
*Tie, name=Constraint-1, adjust=yes
_PickedSurf11, _PickedSurf50
** Constraint: Constraint-2
*Tie, name=Constraint-2, adjust=yes
_PickedSurf13, _PickedSurf51
*End Assembly
** MATERIALS
*Material, name=Bond-coating
*Elastic, Type=Traction
5E4, 10E4, 10E4
*Damage Initiation, Criterion=MaxE
6e-4, 4E-4, 4E-4
*Damage Evolution, Type=Displacement, Softening=linear
**Equivalent total displacement
3E-4
*Material, name=Bond-substrate
*Elastic, Type=Traction
5E4, 10E4, 10E4
*Damage Initiation, Criterion=MaxE
```

```
6e-4, 4E-4, 4E-4
*Damage Evolution, Type=Displacement, Softening=linear
**Equivalent total displacement
7E-4
*Material, name=Coating
*Conductivity
 0.2,
*Elastic
52100., 0.17
*Expansion
 5e-06,
*Material, name=Polymer
*Conductivity
 0.2,
*Elastic
2170., 0.4
*Expansion
 5e-06,
*Material, name=Substrate
*Conductivity
 0.2,
*Elastic
70000., 0.33
*Expansion
 2.5e-05,
** BOUNDARY CONDITIONS
** Name: BC-1 Type: Displacement/Rotation
*Boundary
_PickedSet14, 1, 1
_PickedSet14, 2, 2
_PickedSet14, 6, 6
** Name: BC-2 Type: Displacement/Rotation
*Boundary
_PickedSet52, 1, 1
_PickedSet52, 6, 6
** ----------------------------------------------------------------
** STEP: CoolDown
*Step, name=CoolDown, amplitude=RAMP
*Coupled Temperature-Displacement, creep=none, steady state
0.2, 1., 1e-05, 1.
** BOUNDARY CONDITIONS
** Name: BC-3 Type: Temperature
*Boundary
_PickedSet53, 11, 11, -150.
```

```
** OUTPUT REQUESTS
*Restart, write, frequency=0
** FIELD OUTPUT: F-Output-1
*Output, field, frequency=99999
*Node Output
CF, NT, RF, RFL, U
*Element Output, directions=YES
E, EE, HFL, LE, PS, S, THE, VS
*Contact Output
CDISP, CSTRESS
*Output, field
*Node Output
NT, U
*Element Output, directions=YES
SDEG, TEMP, DMICRT
** HISTORY OUTPUT: H-Output-1
*Output, history, variable=PRESELECT
*End Step
```